Fracture mechanics of concrete: Structural application and numerical calculation

Edited by

George C. Sih

Lehigh University,
Institute of Fracture and Solid Mechanics,
Bethlehem, PA 18015, USA

A. DiTommaso

University of Bologna
Bologna, Italy

1985 **MARTINUS NIJHOFF PUBLISHERS**
a member of the KLUWER ACADEMIC PUBLISHERS GROUP
DORDRECHT / BOSTON / LANCASTER

M. ELICES

5

Fracture of steels for reinforcing and prestressing concrete

5.1 Introduction

This chapter presents an ordered account of the available information on the fracture of steels used for reinforcing and prestressing concrete. Such information is essential to an understanding of the fracture behaviour of reinforced concrete. Reasons of limit space prevent a state of the art survey but, from the literature and references cited, it should be possible to obtain a global view of the current status of the field.

Any study of the fracture of reinforced and prestressed concrete requires not only a knowledge of the characteristic properties of the constituent components, steel and concrete, but also of the behaviour of their interface since it is the bond between the two which governs their interaction. In fact failure of a structural member may be due not to fracture of the steel or concrete but rather to a break down in the interfacial bond. Once again limited space prevents coverage of bond behaviour, even though it is fundamental to a complete understanding of the fracture of concrete. The interested reader might, however, consult the proceedings of the recent conference on Bond in Concrete [11] which cover a wide spectrum of the available knowledge on this subject.

First of all a brief description of the steels used in reinforcing and prestressing concrete is given. Different types of fracture in reinforcing steels are considered next and the importance of defects, principally surface, are discussed. There is very little available information relevant to the case of surface defects since these generally require a three dimensional treatment. Recent solutions to such problems have employed sophisticated numerical techniques, and since reinforcing steels generally fail after appreciable plastic deformation an elastoplastic analysis would be required. This and the three dimensionality of cracks (which tend to originate in the interior) make a quantitative treatment extremely difficult. For this reason the first part will be essentially descriptive. The chapter ends with two sections devoted to the initiation and growth of subcritical cracks; one considers fatigue phenomena, which are of in-

creasing importance in design, and the other environment sensitive cracking which is of increasing interest as construction takes place in more aggressive conditions and with higher design stresses.

The theme of this chapter has now begun to have sufficient coherence to form a branch within the study of the fracture mechanics of civil engineering materials. There are, however, many gaps which are still to be bridged and these are identified within the text. Previously unpublished information is also presented.

Steels for concrete reinforcement. On its own, concrete has a high compressive strength but relatively little resistance to tension and bending. These deficiencies in the tensile and bending strengths may be overcome by the addition of steel reinforcement. The reinforcing steel must have not only adequate tensile properties but also develop a strong bond with the concrete since load is transmitted to the steel through shearing stresses at the interface. This bond which is purely mechanical arises from surface roughness and friction between the steel and concrete.

Steels used in the reinforcement of concrete may be classified according to the method of production as: hot rolled, cold worked or special steels (eg. hardened and tempered steels). In the hot rolling process, the steel is passed through a series of rolls which appreciably reduce the cross section of the steel. In doing so, the comparatively coarse grains of the steel are deformed. The resulting refinement and homogeneity of the metallurgical structures are proportional to the amount of rolling.

Hot rolled mild steel bars may have either a plain or deformed surface while high tensile bars tend to have a deformed surface produced during hot-rolling and consisting of a transverse rib pattern with or without a longitudinal rib.

High strength may be achieved through subsequent cold working of hot rolled bars. The cold working process is usually performed by twisting round ribbed or square bar and controlling the pitch to give optimum strength and bond characteristics.

Steels for prestressing concrete. Prestressing of concrete structures is used to put the greater part of the cross-section of concrete into permanent compression and allow more effective use of the material under externally applied loads, particularly in bending. There are two general types of prestressing: Pretensioning is a method of prestressing in which the tendons are stressed before the surrounding concrete is cast, whereas in post-tensioning the tendons, usually in pre-formed ducts, are stressed after the surrounding concrete has set and hardened.

Because the tendon forces necessary to put massive cross-sections of concrete into the required degree of compression are very large, very high strength steels are often used for tendons and also for some parts of the

anchorage systems. High-tensile steel for prestressing usually takes one of three forms: wires, strands or bars.

Cold drawn wires and strands have a carbon content of about 0.8 per cent (eutectoid) which is mainly responsible for their high tensile strength. The usual manufacturing process involves heating to a temperature in the austenite region, followed by an appropriate cooling procedure to give a metallurgical structure suitable for subsequent cold working. Strength is further improved by cold working carried out by drawing the wire through a series of dies. A final stress relieving heat treatment is given to improve some of the mechanical properties. The stress relieving treatment may be performed under prescribed conditions of deformation to improve stress relaxation.

Smooth and deformed high tensile alloy steel bars and wires are available for prestressing. They are made from high carbon alloyed steel or from medium carbon silicon chromium steel. Bars are hot rolled and generally cold stretched to raise the yield point and to render the bars more linear elastic at stress levels below the yield point. After cold stretching they are frequently stress relieved to improve the ductility and stress-strain characteristics. Steel wires and bars of the silicon chromium type are hot rolled to their final surface condition and then quenched and tempered. Figure 5.1 shows possible shapes of hot rolled deformed bars.

In both pre-tensioning and post-tensioning, the most common method for stressing the tendons is jacking. In post-tensioning, jacks are used to pull the steel with the reaction taken against the hardened concrete; in pretensioning, jacks pull the steel with reaction against end bulkheads or moulds. It is not possible to compile all the systems of prestressing, new systems are being developed and existing ones modified from time to time. Nevertheless, as most steel fractures occur during tensioning, it is expedient to review some of these systems:

The anchorage for the BBRV system is arranged by passing each wire through a hole in a special block and then forming a button-head at the end of the wire by upset cold forging. The wires are cut to the required tendon length before the buttonheads are formed. The buttonheads are located in shaped depressions on the back of the anchorage block.

The PCS Freyssinet system generally uses multi-wire cables or strands. The anchorage system involves passing the strands through a tapered female cone, into which the male cone is forced at the time of jacking and stressing. The conical surface of the male cone carries fluted grooves, and each strand is gripped in a groove as it is stressed and the male cone is embedded in the female anchorage plate.

The CCL anchorage system involves passing the wires through holes in the anchorage block and the swaging of barrel-and-cone wedge grips onto individual strands behind the blocks at the time of stressing.

The anchorages at the end of each bar are provided, generally, by

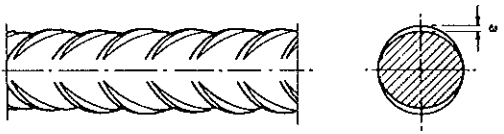

Round deformed rod, hot rolled.

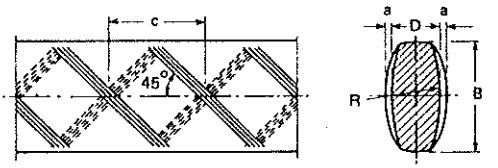

Oval deformed rod, hot rolled.

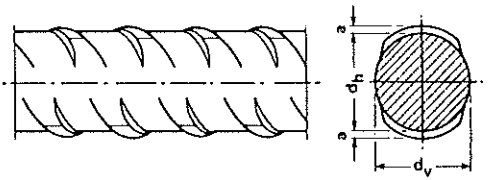

Round deformed bar, hot rolled.

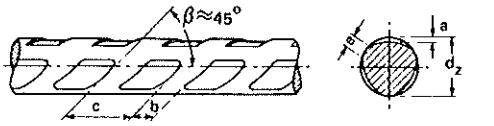

Indented wire, cold drawn.

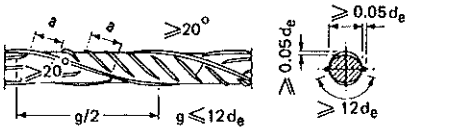

Round deformed bar in twisted condition.

Fig. 5.1. Possible shapes of hot rolled deformed bars. (Courtesy FIP [37]).

threaded assemblies with a nut bearing onto an end plate. Stressing is carried out by hydraulic jacks gripping the threaded end behind the nut and loading onto stools over the end plate. An essential point is the proper threading of the ends to take a special nut capable of developing as nearly as possible the full strength of the bar. By using tapered threads, about 98% of the bar strength is developed.

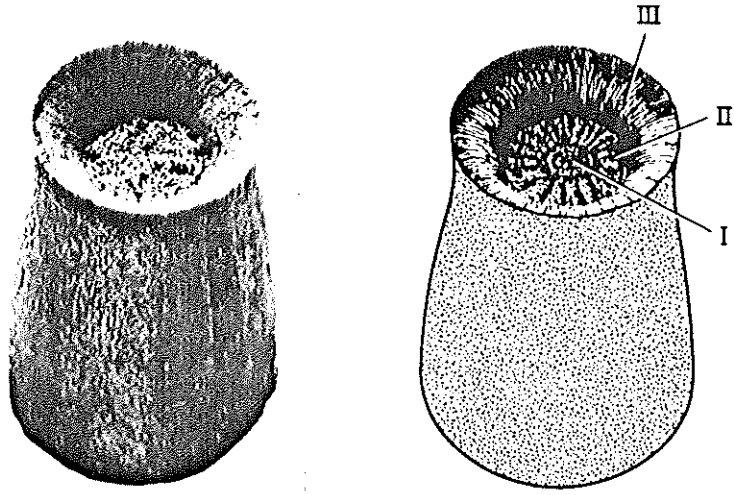

Fig. 5.2. Schematic illustration of cup-cone fracture.

5.2 Fracture

Tensile loading for unnotched specimens. In both reinforced and prestressed concrete the loading made in the reinforcement is one of tension. However, in practice, tendons can be subjected to transverse forces arising from contact or, in the case of prestressing reinforcement, forces from the jack during tendon stressing. This complex stress state can induce rupture and this is discussed at the end of the section. Consider first, however, the simplest case of a wire or rod under tension.

The basic features of ductile fracture that should be modeled in an analysis of tensile bars have been discussed by G.C. Sih [74–76]. Evidence from the fracture surfaces of broken specimens shows that there are three distinct stages of fracture development, each of which possesses a different surface appearance and instability at the macroscopic level. These stages are designated as I, II and III in Figure 5.2. Fracture originates inside region I which represents slow or stable crack growth. It then changes to rapid or unstable crack propagation indicated by region II. Final separation of the material begins as the crack turns away from the normal to the free surface. This slanted fracture surface is usually referred to as the shear lip zone III. The boundary separating stages I and II represents a transition from slow to rapid fracture, while the time elapsed between stages II and III is so short that the load and deformation do not change appreciably during this period. Details and comments on crack propagation beyond elastic limit and shear lip formation are given in [75], where the three-dimensionality of these phenomena is emphasized.

The microscopic aspects of these fractures, at ambient temperatures and under moderate rates of loading, are well documented [64]. The most frequently observed fracture in the smooth bar tensile test, occurs as a result of void nucleation, growth and linkage, following the formation of the central crack. Acting as an internal notch, this crack tends to concentrate the deformation at its tip in narrow bands of high shear strain. These shear bands are at angles of 50° to 60° to the transverse direction. Under the combined action of the tensile stress and the resulting shear strain, "sheets" of voids are nucleated in these bands, growing and elongating until coalescence occurs, producing local fracture of the "void sheet". The crack zigzags back and forth across the plane of the minimum section by void sheet formation as it extends outward radially, reducing the unfractured section of the specimen. This crack grows in a direction perpendicular to the axis of the specimen until it approaches the surface of the specimen. When instability occurs, it then propagates along localized shear planes at roughly 45° to the axis to form the "cone" part of the fracture. Some typical cup-cone fractures of steels for reinforcement and prestressing concrete are shown in Figure 5.3.

The mechanism of the final cup-cone fracture of ductile tensile bars is not well understood. Recently, an analysis of this instability based upon the mechanics of progressive rupture and the tearing modulus concept was suggested by Paris and coworkers [56,48]. As fracture instability is approached, the specimen is fully plastic in the necked region around the crack and the flow stress on the remaining ligament is nearly constant. Crack propagation decreases the area of remaining uncracked ligament and lowers the plastic limit load. Assuming fixed grips, this results in a certain amount of elastic shortening of the unnecked portions of the specimen. During the instant of unstable fracture, the movement of the testing machine grips is nearly zero, and thus the total length of the specimen remains nearly constant. Therefore, for an increment of crack growth, if the amount of elastic shortening is greater than the amount of plastic elongation associated with crack growth then instability results. When the amount of plastic elongation and elastic shortening are equated, then all intrinsic material properties, as distinguished from properties of geometric configuration of the specimen, can be separated to different sides of an equation. The side of material properties is termed T_{material} while the side of geometric configuration is termed T_{applied} [56]. Kong and Paris found, for a round tensile bar of length L diameter D, with a circular center crack of diameter $d = 2a$.

$$T_{\text{material}} = \frac{\mathrm{d}J}{\mathrm{d}a}\frac{E}{\sigma_0^2} \leqslant \frac{4Ld}{D^2} = T_{\text{applied}} \tag{5.1}$$

where σ_0 is the most appropriate flow stress. Also, the tearing instability

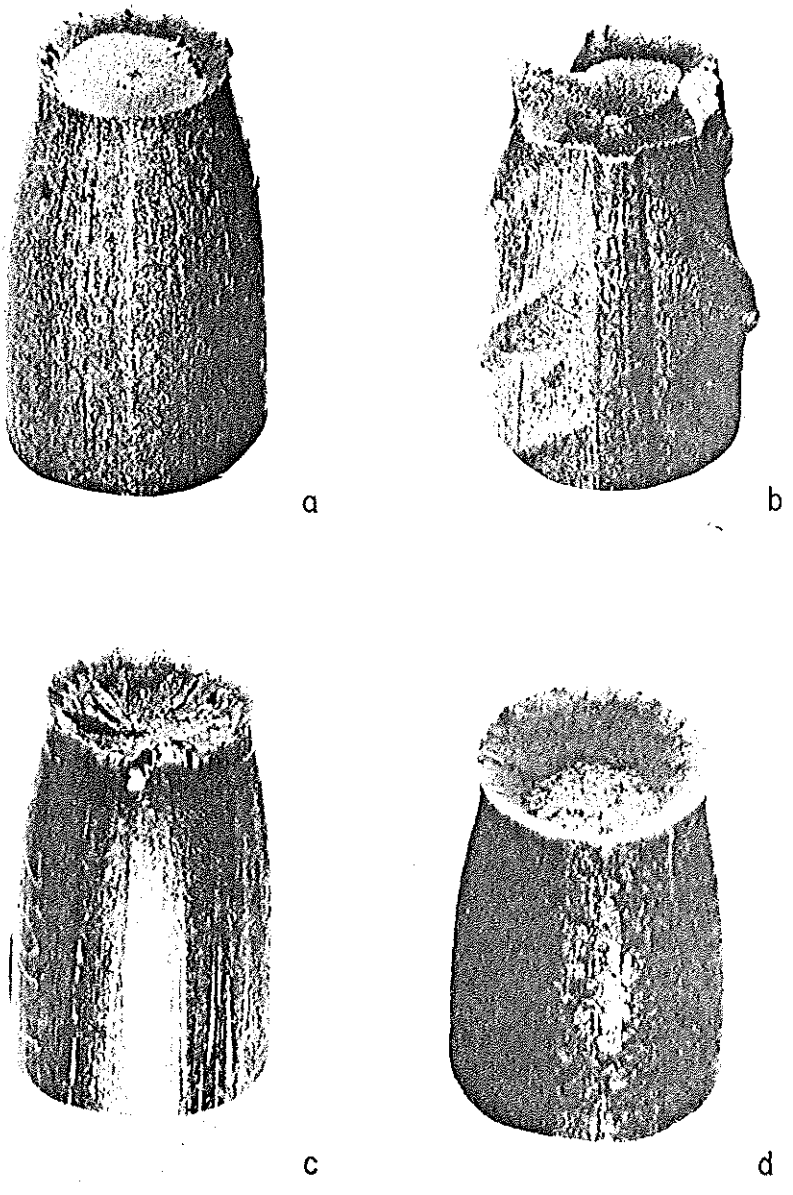

Fig. 5.3. Typical cup-cone fractures. Reinforcing steel; a – smooth, b – deformed steel for prestressing; c – cold drawn; d – quenched and tempered.

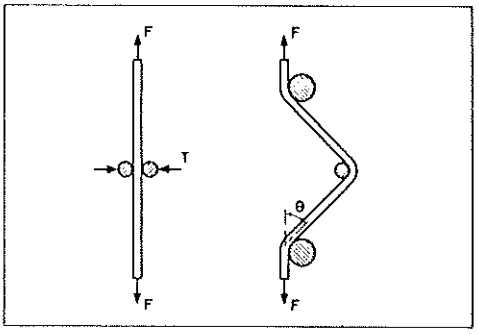

Fig. 5.4. Tensile tests with lateral constriction.

of a single microflaw in uniform plastic stress field can be obtained [48]:

$$T_{\text{material}} = \frac{\mathrm{d}J}{\mathrm{d}a}\frac{E}{\sigma_0^2} \leqslant 2.6 = T_{\text{applied}} \tag{5.2}$$

In consequence, after a certain amount of deformation, a microflaw, in the center of a tensile bar might begin to grow (in particular the beginning of growth might be associated with J_{IC} or a similar parameter). If growth begins and T_{material} is less than 2.6, Equation (5.2) implies instability from the beginning of growth and perhaps a sudden completely flat fracture occurs, a so-called star fracture. However, if T_{material} is greater than 2.6 Equation (5.2) implies that microflaw growth will at first be stable. But as the crack grows, its diameter d increases and Equation (5.1) implies that at some point T_{applied} may respondingly increase to exceed T_{material} and instability should ensue. Since the slip field associated with Equation (5.1) is 45° slip from the crack tip to the outside of the bar, this instability mechanism accounts for the change from flat stable growth to oblique-shear, forming the cup and cone.

As mentioned at the beginning of this chapter, the usual fracture of reinforcing and prestressing steel wires is of the cup and cone type. However, inside the anchorages and in places associated with a lateral compression a shear type fracture may occur, with an important lowering of the fracture load [37,42,51]. This type of rupture has been reproduced in the laboratory by Maupetit et al. [51], as well as by the author and coworkers, during tensile tests with a transverse load or by deviating the wire, as shown in Figure 5.4. The wires tested were made of bainitic, oil quenched and tempered and cold drawn carbon steels. Only the last type of steel exhibited shear fractures. A marked decrease of the fracture load as the lateral compression increases can be seen in Figure 5.5. Francois et al. [51] conclude that this test may be used to characterize the resistance

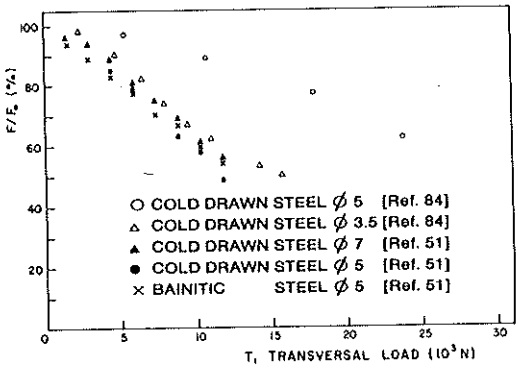

Fig. 5.5. Tensile strength under lateral load, [51], [84].

of wires to shear fracture and also for selection, or quality control, of steel wires for some prestressed concrete applications.

Bending [42] for unnotched specimens. The bend test, which is used to determine the ductility of wire, is designed to subject the test specimen to a large amount of deformation. Such tests are standardized. Under test conditions, the tensile strain on the outer surface of the wire is very high, 50% when the diameter of the mandrel equals the diameter of the wire. Steel wire that has an elongation of only 2% as measured in the conventional tensile test, may withstand such bending without fracturing. The usual bend test is made by bending the test specimen back and forth over mandrels considerably larger than the wire diameter. Such tests have shown that the number of reverse bends has a well defined relationship to the true strain at the point of fracture in the tensile test [41]. The bend test on steel wire also correlates with the reduction of area as measured in the tensile test [40].

The fact that steel wire will elongate as much as 50% in the bend test without necking-down is due to the stress distribution in the bend test. Only one side of the specimen is under tension while the opposite side is subject to compressive stress. While the tensile side is trying to neck, the compression side is trying to increase in cross-section. The end test is considered to be a good measure of quality because the maximum tensile strain takes place on the surface of the wire where defects are most likely to be present.

Torsion [42] for unnotched specimens. The torsion test has been used in the wire industry for evaluating the uniformity of wire. In contrast to the tensile test, the shearing stress in the torsion test is equal to the tensile

stress, for this reason the fracture generally takes place on a plane of maximum shearing stress.

During some tests, after only about one twist, a sudden decrease in torque may be registered due to the formation of a longitudinal split in the wire parallel to the wire axis. If the test had been interrupted at that point, and a transverse section made through the split, examination would have shown that the split extended from the surface down to a point approaching the axis of the specimen and a very irregular torque-twist curve is developed until the final fracture takes place.

Another type of fracture is the helical fracture, generally found in specimens that fracture initially with a transverse shear fracture. The helical fracture is believed to be the result of the sudden release of torque after the initial fracture and the subsequent impact load on the remaining part of the test specimen.

The quality of steel wire is normally evaluated by the number of torsions to failure. The stress distribution in the torsion test is significantly different from that of the tension test and, because of this stress condition, the quality of the wire surface can considerably influence the test results.

Theoretical approach for notched specimens. Brittle fractures are sometimes observed in steels used to reinforce or prestress concrete. These are characterized by little or no deformation before fracture and are usually initiated at some surface defect; perhaps a notch or crack caused by fatigue or stress corrosion. In these cases the failure load can be well below the elastic limit so that, as mentioned above, the deformation may be very small. Consequently this type of fracture is very difficult to anticipate. In this section, the theoretical approach to the simplest cases is summarised and, then, results from laboratory tests are discussed.

The case of a surface crack in a linear elastic regime is considered first. The treatment is then extended over cover elasto-plastic behaviour. A summary of most of the information summarised below may be found in three civil engineering doctoral theses (Astiz [4], Athanassiadis [7] and Valiente [82]).

The investigation of numerous fractures which have occurred in service, as well as in laboratory tests, suggests the defects which initiated failure probably had a thumb-nail shape and that they may be of two types. The first pertains to cracks with a more or less elliptical boundary and the second to shallow cracks which extends around the circumference of the cylinder.

A number of crack shapes are illustrated in Figure 5.6. The treatment of such cracks can then be simplified by comparing the shapes to elliptical areas which are symmetrical with respect to the meridional plane and lie in a plane perpendicular to the edge of the tendon. With the

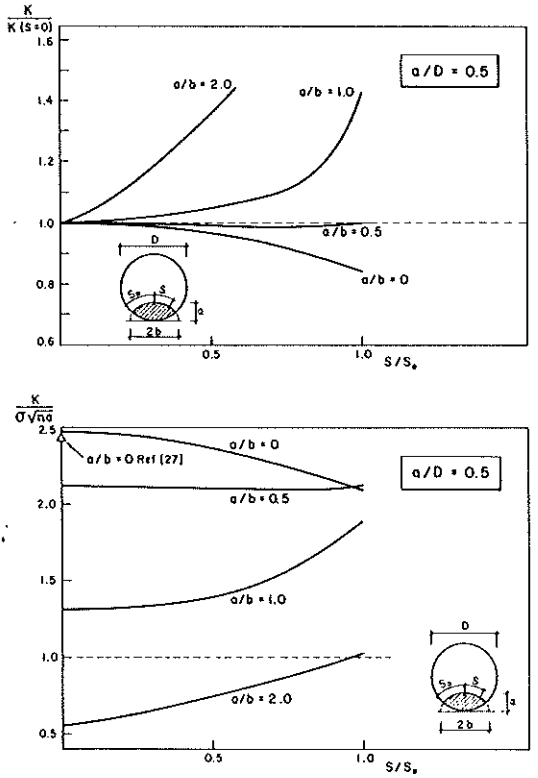

Fig. 5.7b. Variation of the stress intensity factor along the crack border.

(1) The variation of $K_I(\theta)$ with a/b. The maximum value of K_I depends upon a/b. For flat fronted cracks (say $a/b < 0.7$) the maximum occurs in the center, $\theta = 0$, and crack growth would tend to make the front bow outwards. Acute cracks, on the other hand ($a/b > 0.8$), have the maximum values of $K_I(\theta)$ at the edges and subsequent crack growth would be such as to flatten the crack front. It would appear that some values of a/b could give rise to K_I values which are constant along the crack so that growth takes place by the production of similar, iso $-K$, crack fronts.

(2) The variation of $K_I(\theta)$ with a/D. The effect of crack depth on the value of K_I is most pronounced in flat cracks (small values of a/b) than in pointed cracks, for which it is hardly apparent.

Two particular crack geometries have been studied by a number of authors; these are straight-fronted and circular cracks. Some of the published results for these shapes are shown in Figures 5.7a and 5.7b and compared with those obtained from the numerical techniques mentioned above.

Stress intensity factors have been calculated by Blackburn [17] by finite element methods for straight edged crack and found that K_I, due to tensile or bending loads, was highest at the centre and lower than that due to a semi-elliptical notch in a slab of the same thickness under the same load. An average value for the stress intensity factor has been calculated by Daoud [27] from strain energy release rate determinations. Values of G were obtained using a finite-element representation of the bar and by measuring the compliance of the bar experimentally. For crack depths of less that one-half diameter, average K_I are found to be lower than existing results of rectangular bars having the same relative crack length. Also, average stress intensity factors were determined for single-edge-crack solid and hollow round bars loaded in tension by Bush [22]. These factors were calculated from experimental compliance measurements made over a range of dimensionless crack depths from 0.05 to 0.65. A comparison was made with data in the literature for rectangular bars. Results for a round bar falls below that for a rectangular bar, as already noted.

Results for surface cracks of circular shape in cylinders loaded in tension have been obtained by Fan [36] using the alternate method. It is basically an iterative method that couples two solutions; the exact solution for a penny-shaped crack in an infinite elastic body and a series solution for a cylinder with finite size under an arbitrary lateral surface load. From the alternate action of these basic solutions, an analytical expression for $K_I(\theta)$ can be obtained.

Both the finite element and boundary integral equation methods yield numerical results, which, for application, may be presented in tabular or graphical form. The programs give the potential energy P of the cracked wire from the calculation of the displacements and stresses at each node for different crack configurations. The strain energy rate G is deduced from the potential energy as

$$G = \sup\left(-\frac{\delta P}{\delta S}\right) \tag{5.5}$$

δS being a virtual increase of the crack surface. An average value of G deduced from the local values of K_I was also computed as

$$G^* = \frac{1}{2s}\int_{-s}^{+s}\frac{K_I^2}{E'}\mathrm{d}S \tag{5.6}$$

S being, as always, the curvilinear coordinate of a point on the crack front.

Figure 5.8 shows the variation of G with a/b and a/D. It can be seen

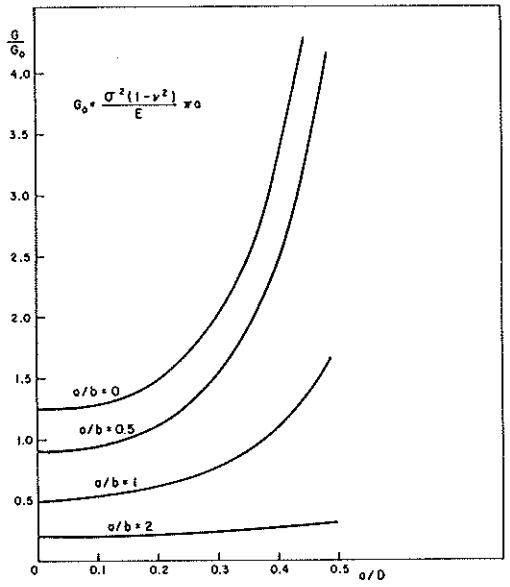

Fig. 5.8. Energy release rate for different crack configurations.

that, for a given crack depth (a/D), the strain energy release rate, G, increases rapidly with the crack shape parameters; being greater for flatter, less curved crack fronts (small values of a/b).

$K_I(\theta)$ and G values for the same crack geometries subjected to bending have also been obtained [6,9,17,22,27,36]. A study by Athanassiadis [7] and Maupetit et al. [51] is of interest since the case of a cracked specimen subjected to lateral forces is considered. This could be particularly useful in account for the stress state within the anchorage zone or for complex loading in general [51,62].

This section, covering theoretical attempts to solve the problem of the fracture of cracked tendons, is concluded with a summary of efforts made at extending the treatment to more realistic situations. In doing so, brief comment on the roles of plasticity and notches will be made.

At ambient temperature steels used for reinforcing and prestressing concrete exhibit some plastic deformation, even in the presence of cracks. While experiments shows that deep cracked cold drawn prestressing steel does behave in a linear elastic manner, both low yield reinforcing steels and quenched and tempered prestressing steels do not obey linear elastic fracture mechanics. For the latter cases, Valiente [84] has developed two limiting solutions; one based on a generalisation of the work of Hahn [46] for pipes and the other on limit analysis.

The crack tip opening displacement may be determined using the

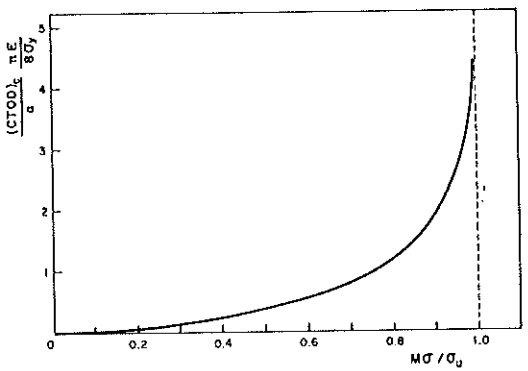

Fig. 5.9. Variation of CTOD as a function of $M\sigma/\sigma_Y$.

Dugdale-Bilby-Cottrell-Swinden (DBCS) model [48]:

$$\text{CTOD} = \frac{8\sigma_y}{\pi E} a.\ \text{ln. sec.}\ \frac{\pi M\sigma}{2\sigma_u} \tag{5.7}$$

in which M is the geometrical factor for an elliptical crack, σ_u is a flow stress whose value is usually taken somewhere between σ_y (the yield stress, if it is well defined) and σ_R the tensile strength and the other notation has its usual meaning. If it can be assumed that crack growth will occur when CTOD reaches a critical value $(\text{CTOD})_c$, and that this is a material property, then the criterion for crack growth can be represented on Figure 5.9. It is then apparent that if the term, $(\text{CTOD})_c \pi E/8a\sigma_y$, is high (either because the crack depth is small or the resistance high), the point on the curve representing the condition for fracture in a given material with a given crack,corresponds to a value of $\sigma M/\sigma_u$ of about one. In these cases the fracture criterion can be taken as

$$M\sigma = \sigma_u \tag{5.8}$$

This result although overextended to cases of large scale plasticity, fits quite accurately with some experimental results.

Valiente's limit analysis solution is based on perfectly plastic behaviour. Equilibrium of forces across the ligament, Figure 5.10, yield the following failure criterion

$$F\sigma = \sigma_y \tag{5.9}$$

where σ is the applied stress, σ_y the yield stress and F is given by

$$F^{-1}\left(\frac{a}{D}, \frac{a}{c}\right) = \frac{2}{\pi} \text{ arc sin}\left(1 - \frac{2z}{D}\right) + \frac{4}{\pi}\left(1 - \frac{2z}{D}\right)\left(\frac{z}{D} - \frac{z^2}{D^2}\right)^{1/2} \tag{5.10}$$

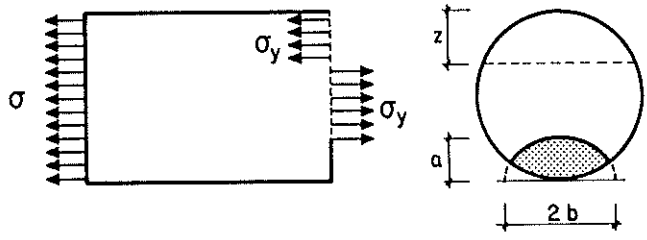

Fig. 5.10. Limit analysis for a cracked bar.

which is obtained from moment equilibrium and z is shown in Figure 5.10.

Another complication which arises when attempts are made to establish failure criteria for more realistic cases is the consideration of the notch root radius. The formulae mentioned above were valid for mathematically sharp cracks. However, unstable fracture is, sometimes, initiated at a notch of finite tip radius. In such cases corrections suggested by Creager and Paris [25] may be used to determine the elastic stress field in the vicinity of the notch. The problem of deriving a failure criterion, however, is not solved since fracture tends to involve significant plastic deformation. It is then necessary to adopt a two parameter approach.

For the sake of completeness and as a reference for future work attention is drawn to fracture toughness measurements made on rectangular notched bars subjected to tensile loading [8,29].

Finally, cold worked steels show a marked degree of anisotropy which results from the fabrication process. It is much easier to propagate cracks in the longitudinal rather than the transverse direction. From the toughness point of view, this is a useful property since cracks tend to deviate from the plane perpendicular to the edge and seek a plane of propagation parallel to the edge. There is a consequent reduction in the stress intensity factor and the crack may even be arrested. Anisotropy adds further complexity to the analysis and, at the time of writing, the author knows of no solution to the problem of a surface crack in a transversely anisotropic cylinder.

Experimental results for notched specimens. In this section various aspects of the stress intensity factor are considered; firstly, the experimental determination and then the critical value at which crack propagation occurs. The only direct experimental determinations of the stress intensity factors for a cracked cylinder are those obtained from the photoelastic stress freezing technique [5,83]. The results from such tests were in broad agreement with those from finite element and boundary integral analyses. Indirect methods involving compliance measurement have also

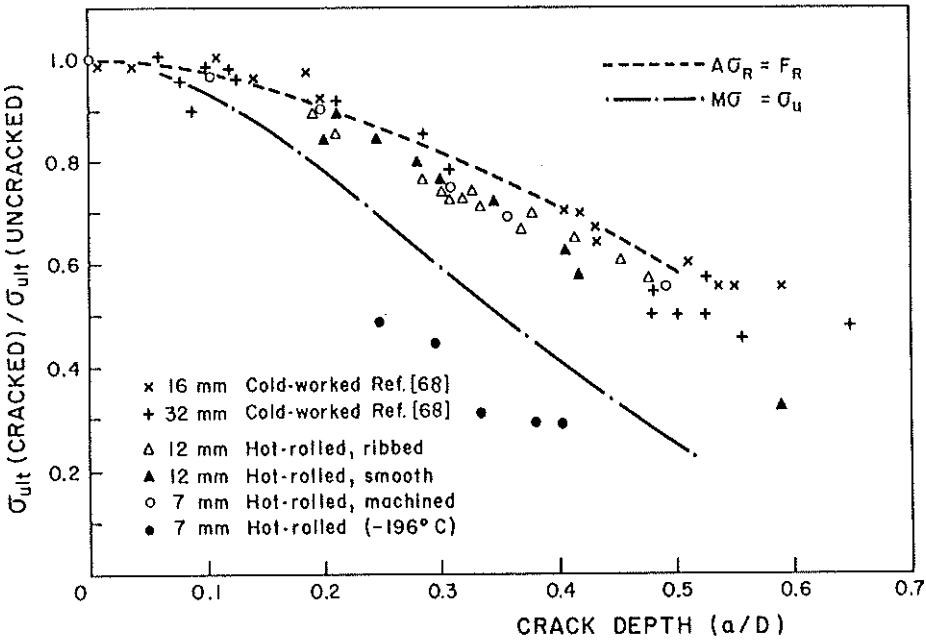

Fig. 5.11. Effect of crack depth on tensile strength.

yielded K_I values which agree well with theory [4,22,27]. Critical values of K_I have been determined from fatigue tests on cracked specimens and the theoretical expressions just described. Fracture toughness values K_c are, thus, available for reinforcing and prestressing steels. This section continues with a discussion of the tensile behaviour of cracked cylindrical specimens taken from such steels.

The simplest and most direct method of evaluating the effect of cracks on the rupture load and ductility consists of performing tensile tests on specimens with different crack depths. Results of such tests on various steels are shown in Figure 5.11 [31,68,82]. The materials tested were, cold worked bars of 16 and 32 mm. diameter and hot rolled smooth and ribbed bars of 12 mm. diameter.

The great toughness of these steels is immediately apparent, that is to say, the presence of small cracks causes little reduction in the failure load. This effect should be borne in mind when the growth of subcritical cracks is considered: say under the action of fatigue loading, stress corrosion or corrosion fatigue. The results of Figure 5.11 can be explained with the aid of models based on the plastic behaviour of the materials. Two extreme solutions have been superimposed upon the experimental results; one, crude approach, assumes that failure occurs when the rupture stress is developed across the whole section area A so

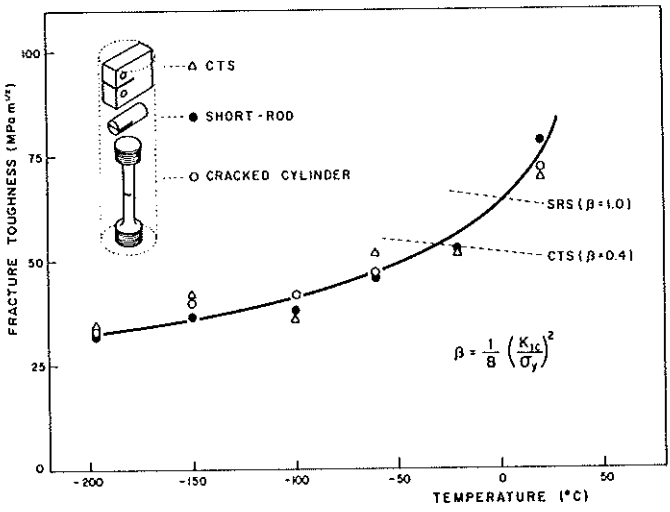

Fig. 5.12. Fracture toughness of hot rolled steel for concrete reinforcement.

that the stress distribution is then uniform. The rupture load F_R is then given by:

$$F_R = \sigma_R A = F_{R0} A / A_0 \tag{5.11}$$

where F_{R0} is the failure load of the uncracked specimen. This provides an upper bound which is not far from experimental values. A lower solution is obtained by extrapolating the fracture mechanics results into the elastoplastic regime using the DBCS model. This gives $M\sigma = \sigma_y$. An intermediate criterion based on limit analysis, for example, would give results which lie between those mentioned above and which are closer to the experimental observations.

If the experiments, described above, are carried out at low temperatures (-196°C) linear elastic behaviour is observed on a force-displacement record. Such behaviour suggests that valid K_{IC} results may then be obtained. Compact tension, short-rod and cracked cylindrical specimens machined from 57 mm. diameter hot rolled steel bars were used to determine the apparent K_{IC} values shown in Figure 5.12 [31,54]. It is clear that, above -30°C, compact tensile specimens do not yield valid K_{IC} results. Short rod specimens can be used to determine K_{IC} up to temperatures of about 0°C.

If it can be assumed that stable crack growth does not occur at low temperatures, so that once initiated cracks propagate rapidly, the linear elastic fracture mechanics expressions for $K_I(\theta = 0)$, using the appropriate geometrical parameters, can be used to estimate the variation

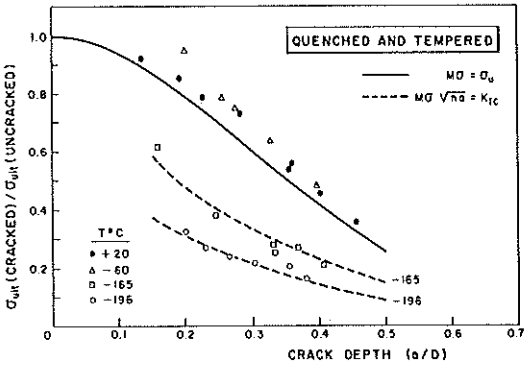

Fig. 5.13. Effect of crack depth on tensile strength. Quenched and tempered steel. $\sigma_y = 1380$ N/mm^2.

of failure load with crack depth. At liquid nitrogen temperature (-196°C) a value of $K_{IC} = 32$ MNm$^{-3/2}$ provides a good estimate of failure loads over the experimental range of (a/D) values.

The same steps, outlined above, are followed in this discussion of the behaviour in prestressing steels. Quenched and tempered steels are considered first and then cold drawn steels.

Figure 5.13 illustrates the variation of normalised values of rupture load with crack depth at temperatures ranging from ambient down to -196°C. These results were obtained from tests on quenched and tempered tendons with a 9 mm. diameter and a 0.2% proof stress of 1380 N/mm^2 [31,54,82].

For temperatures down to -60°C it will be observed that results fit an elastoplastic failure criterion $M\sigma = \sigma_u$ even though the steels have a high yield stress and exhibit little plastic deformation. At very low temperatures, the usual fracture mechanics expressions predict the failure loads, at least, within the experimental range of (a/D).

With a view to determining a valid K_{IC} value, liquid nitrogen temperature experiments were performed on short-rod specimens taken from the longitudinal direction in 9 mm. tendons and also on conventional cylindrical specimens. Values of $K_{IC}(L) = 29$ MNm$^{-3/2}$ and $K_{IC}(T) = 39$ MNm$^{-3/2}$ were obtained; where L refers to the longitudinal and T to the transverse direction. The difference in the values suggests a weak anisotropy. The variation of fracture toughness in the longitudinal and transverse directions with temperature is shown in Figure 5.14 [31,54]. Plane strain fracture toughness values for longitudinal specimens are considered to be valid up to a temperature of -150°C. The $K_{IC}(T)$ values were obtained using the techniques described in the previous section while $K_{IC}(L)$ values were determined following Barker's recommended proce-

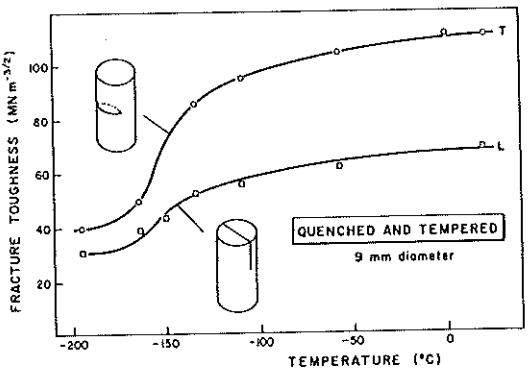

Fig. 5.14. Fracture toughness of quenched and tempered steel for prestressing concrete.

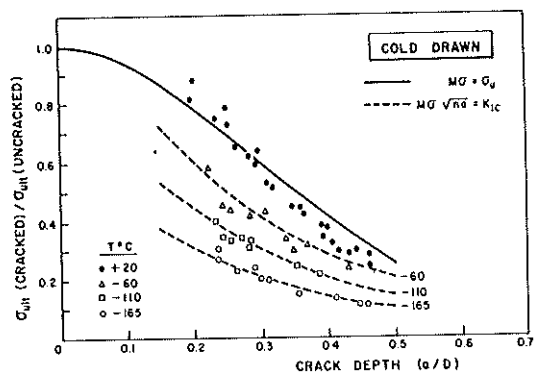

Fig. 5.15. Effect of crack depth on tensile strength. Cold drawn steel. $\sigma_y = 1590$ N/mm^2.

dure [12]. The range of validity of transverse specimens is less than for longitudinal ones.

Analogous results for cold drawn eutectoid steels of 7 mm. diameter and 0.2% proof stress $\sigma_{0.2} = 1590$ MNm$^{-3/2}$ are shown in Figures 5.15 and 5.16 [31,54,82]. This material exhibits a greater degree of anisotropy which arises from the fabrication procedure. This frequently results in a mode of rupture in which the crack tends to leave the plane perpendicular to the edge and propagate in a longitudinal direction. Tensile fractures for quenched and tempered (little anisotropy) and cold drawn wires are compared in Figure 5.17. The strong anisotropy makes interpretation of experimental results more difficult for cold drawn wires but Figure 5.15 does suggest that the $M\sigma = \sigma_u$ criterion can be used at ambient temperature and that, at low temperatures, linear elastic fracture mechanics may be applied, at least, for $a/D > 0.15$. Fracture toughness values for longitudinal and transverse cracked specimens are shown in Figure

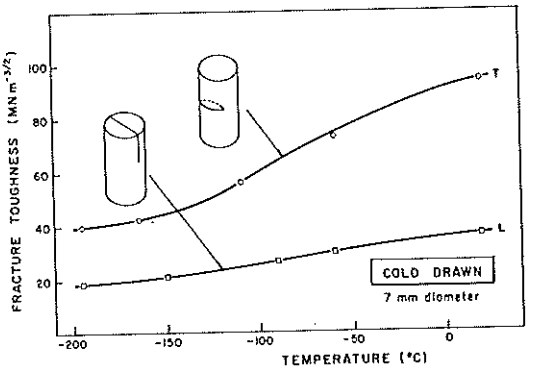

Fig. 5.16. Fracture toughness of cold drawn steel for prestressing concrete.

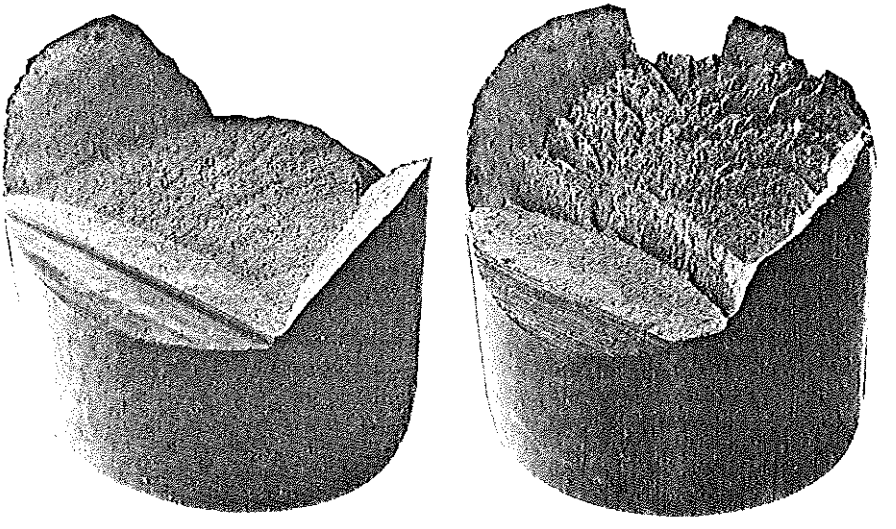

Fig. 5.17. Tensile fractures of cracked wires for prestressing concrete. (left) quenched and tempered. (right) cold drawn.

5.16. Longitudinal values may be valid upto $-60°C$. There does not seem to be the marked transition which was obtained with quenched and tempered steel. It should be remembered, however, that the results are based on expressions for isotropic materials and that crack propagation tended not to be confined to the plane perpendicular to the edge. Other attempts to measure the fracture toughness of cold drawn wires have been made by McGuinn [52,53].

5.3 Fracture under extreme conditions

Parameters such as strain rate and temperature are known to affect the fracture behaviour of reinforcing and prestressing steels. In this section, the effects of extreme values of these parameters are discussed. Such extreme values may occur when a structure is subjected to impact loading, in the case of strain rate. Fires or storage of liquid natural gas in prestressed concrete are examples of extreme temperatures conditions.

Effect of strain rate. Very few, well documented, tests on the influence of strain rate on the fracture behaviour of reinforced concrete are available. Results of tests carried out on reinforced concrete structures under static and dynamic loads show that the behaviour is mainly influenced by the properties of the steel under test. Most of the case studies available have been based on reinforced concrete, this is why the behaviour of reinforcing steel is better understood. The investigations were performed on service steels and there is no data on the cracked or notched dynamic response. It is known that if steel specimens are surface machined for the application of strain gauges it is difficult to obtain realistic values of strain distribution. Tests performed by Limberger et al. [50] at different strain rates showed significant differences in permanent strain distribution after fracture along lightly machined specimens and others which were ribbed.

The few available results [2,47,77] allow the following general comments to be made upon the ductility. Cold worked reinforcing steels exhibit an unexpected behaviour. Increasing the loading rate increases the elongation. This phenomenon is much less marked in hot rolled steels. The effect of strain rate upon the stress strain curves of a number of steels is illustrated in Figure 5.18. Prestressing steels suffer a loss of ductility of between 15% and 20% [2]. The reduction in area decreases for all types of steel as the strain rate increases but the reduction is small being of the order of 2% to 5%.

As far as the relationship between strength and strain rate is concerned, a slight increase has been observed with increasing strain rate in the range $\dot{\varepsilon} = 5.10^{-5}$. Reinforcing steels show a 10% increase in the limit of proportionality and in the elastic limit but the increase in the rupture load is somewhat less at about 5%. Increments for prestressing steels are still less, between 2% and 4%.

Experiment has shown that the ductility parameters (uniform and permanent elongation after rupture) and strength (limit of proportionality, yield and stress and failure load) are related to the strain rate through a logarithmic law over the range $\dot{\varepsilon} = 10^{-5}$ to $10\ s^{-1}$,

$$a = A + B \log \dot{\varepsilon} \tag{5.12}$$

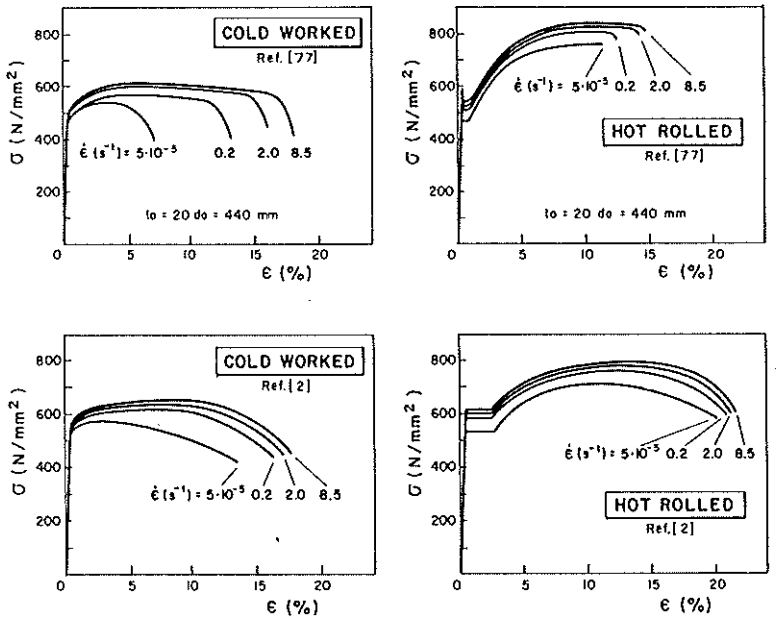

Fig. 5.18. Stress-strain curves at different strain rates. Influence of the quality of the steel.

where a represents one of the parameters mentioned above and A and B are material properties of the steel. It is also possible to use an expression which has only one dependent variable C[2] of the form

$$\frac{f_{dyn}}{f_{static}} = 1 + C \log \frac{\dot{\varepsilon}}{\dot{\varepsilon}_{static}} \tag{5.13}$$

values of A, B and C are given in the references.

Several tests on reinforced concrete beams have been performed to demonstrate the influence of the steel properties on the behaviour of the tested structure under high strain rates [50]. Beams with a high percentage of reinforcement, both tensile and compressive, failed by fracture of the reinforcement in the tensile zone. The concentration of cracks in the plastic hinge implies a high strain concentration in the reinforcement. The increase of the inelastic strains in dynamic beam tests is as significant as that in the tensile tests with increasing strain rate. The ductility, as measured in a bending moment-rotation diagram, of beams reinforced with cold drawn steel increases significantly with the rate of deflection, whereas the beam reinforced with hot rolled steel are rather insensitive to the rate of straining.

The properties of the reinforcement matrix interface over a range of

strain rates is also required for prediction of the fracture behaviour of reinforced concrete structures [63,77]. To study the influence of rate of straining on the bond strength between the reinforcement and concrete pull-out tests have been performed. No significant influence of straining rate on bond strength was observed for plain bars and prestressing strands. However deformed bars showed a significant increase in bond strength with loading rate. The rate effect was also found to be greater for low strength concrete specially at small displacements between reinforcing steel and concrete. This result can be interpreted such that the effective bond length of a deformed bar decreases with increasing loading rate. This rate sensitivity of deformed bars is believed to occur also because of the bearing of the ribs on concrete which produces crushing and splitting of the concrete which is expected to be rate dependent.

Effect of high temperature [24]. Fracture properties for all types of steel are affected by temperature. Composition and processes of manufacture affect the behaviour of reinforcing steels. With temperatures of about 350°C recrystallization of the micro-structure commences which leads to a loss of the work-hardening effects. This explains the differences observed between cold-drawn or cold-twisted reinforcement and high tensile alloy steel.

Two types of tests are carried out which attempt to reproduce the mechanical conditions of the reinforcement in concrete elements under fire attack; stress-strain tests at the desired temperature, by this method the temperature dependent rupture strength can be measured, and creep tests to measure the critical temperature, at which $\dot{\varepsilon} \simeq 10^{-4}\ s^{-1}$. Rapid elongation of the steel at the critical temperature normally leads to undue rate of deflection and subsequent collapse of the structural member.

For design purposes the maximum strength, may be taken from Figure 5.19 as recommended by CEB [24].

Similarly, the benefits of the thermomechanical treatment of prestressing steels disappear when the treatment temperature is again reached. This explains the differences in the performances at high temperatures of cold-drawn stabilized steel and quenched and tempered steel of the same original strength.

Figure 5.19 shows the decrease in ultimate tensile strength of prestressing steels when the temperature increases. Two curves, which may be considered to be boundary values for the tensile strength have also been included for design purposes.

To predict fracture of reinforced concrete at elevated temperatures, the behaviour of concrete, reinforcing steel and prestressing steel has been investigated. In comparison with the knowledge accumulated for these materials little is known about bond at high temperature. An extensive experimental study has been initiated by Rostasy and co-

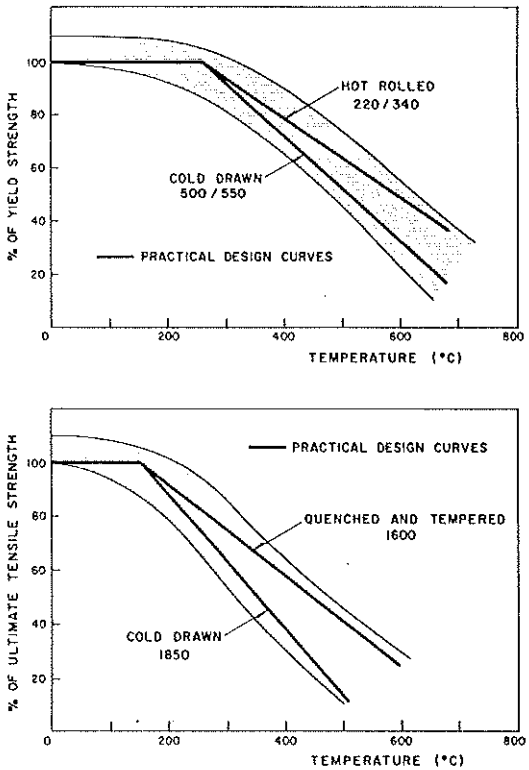

Fig. 5.19. Influence of temperature in tensile strength. Ref. (24).

workers [66,67]. The test results can be applied to estimate the safety of a bond anchorage against slip failure. It is possible to relate the load-displacement relationship τ, Δ from a bond test, to the compressive strength of concrete, β_w

$$\frac{\tau(T)}{\beta_w(T)} = A + B\Delta^C \tag{5.14}$$

where the bond stress has been subdivided into an adhesive resistance and a shear resistance. The adhesive resistance A disappears as the temperature exceeds 300°C. The coefficients B and C, describing the shear resistance, are independent of the compressive strength. Thus the bond stress is proportional to the strength of concrete, as the temperature rises. From this expression the distribution of bond stresses along the anchorage length of a bar and the safety against slip failure in case of fire can be determined.

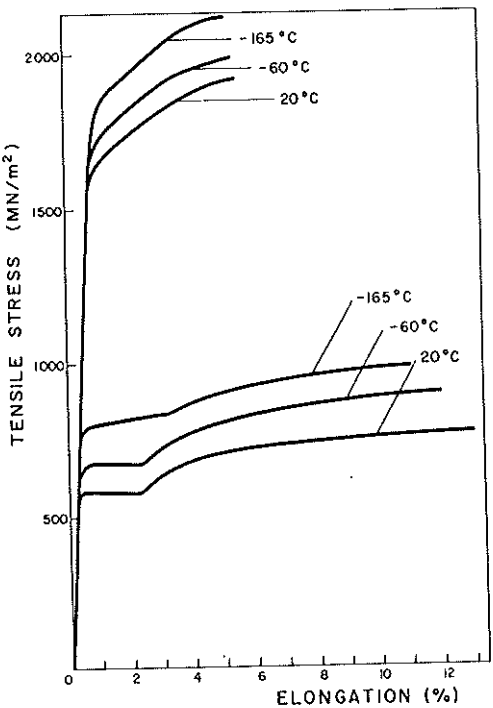

Fig. 5.20. Stress-strain diagrams of steels for reinforcing and prestressing's concrete, at different temperatures.

Effect of low temperatures. Prestressed concrete is a material normally used at ambient temperature conditions but it can also be used structurally at cryogenic temperatures. The satisfactory performance of prestressed concrete in cryogenic environments, coupled with its inherently sound structural characteristic, makes this material ideally suited to a variety of applications in the storage of cryogenic liquids. A state of the art report on the behaviour of prestressing steel and systems, reinforcing steel and concrete at low temperatures has been recently published, Elices, Faas, and Rostasy [33] in which some information relative to steel fracture has been included.

Tensile tests on unnotched samples have shown that steels for prestressing and reinforcing steel exhibit an increase in ultimate tensile strength as the testing temperature is reduced. This behaviour is depicted in Figure 5.20. It can be seen that, the elongation is not appreciably reduced.

A cause of concern, in the use of these steels at low temperatures, is the possible sensitivity to the presence of cracks and notches. This behaviour has been illustrated in Figure 5.11, for reinforcing steel, at

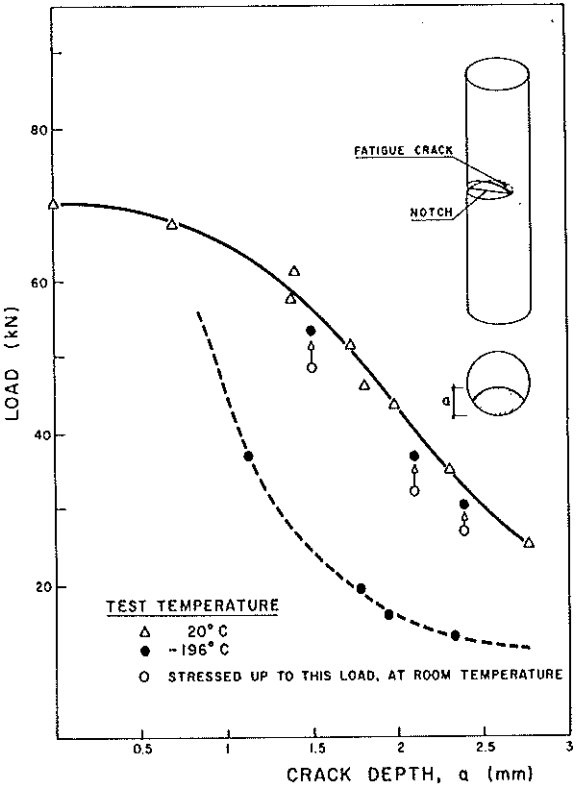

Fig. 5.21. Effect of prestretching before cooling.

−196°C, and Figures 5.13 and 5.15 for different types of prestressing steel. Fracture toughness has also been measured and results are shown in Figures 5.12, 5.14 and 5.16. In spite of its decrease at low temperatures steel tendons are tough enough, since the tendons are stretched at ambient rather than at very low temperatures. The behaviour which should be simulated in laboratory tests is that of a cracked tendon stretched at ambient temperature and subsequently loaded. The results of such an experiment are shown in the Figure 5.21 and it can be seen that a reasonable toughness is still achieved.

As already mentioned, for the design of bond anchorages and also for crack control, the bond strength, as well as the bond stress-displacement relation, must be known. Although many tests have been done at room temperature, only few tests have been performed at low temperatures [43,86].

Tendon anchorages are sensitive zones where fracture may be produced and this risk may be increased at low temperatures. For cryogenic applications it is important to note that, whether or not the cold strength

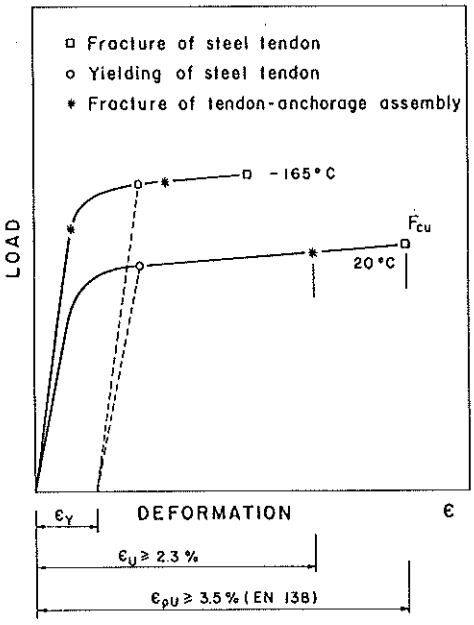

Fig. 5.22. Requirement for tendon-anchorage assembly (Ref. 33).

of the prestressing tendon is utilized in structural analysis, the tendon anchorage assembly does not fail in a brittle fashion. This means that the failure load of the tendon-anchorage assembly, for any value of the temperature, should exceed the cold yield strength of the prestressing steel. This basic requirement is shown in Figure 5.22. A failure load below the yield strength is accompanied by a brittle type failure.

5.4 Fatigue

Although fatigue of reinforced and prestressed concrete has not proved to be a problem in the past, the fatigue lives of many future structures will require assessment. The reasons for this are: (1) Refinements in the method of structural analysis and load evaluation, which imply reduction of safety factors and allowable live loadings (2) improved tensile strength of reinforcing steels not being accompanied by a similar improved fatigue strength and (3) the growing use of prestressed and reinforced concrete structures which in service are predominantly subjected to loads of repeated nature or aggressive environments that may reduce fatigue strength.

If design is to be based on the fracture of steel tendons, fracture mechanics techniques can be used to predict stress range-life data. These

techniques complement the traditional approach based on SN curves, allowing a distinction betwen initiation and propagation times. Another advantage of the method is that it allows a proper investigation of the effect of any of the different factors which influence the fatigue behaviour of reinforcement; type of bar, mean stress, bar diameter, etc., which has often confused experimental studies. Further, this method has been used to predict the fatigue life of reinforced concrete beams and provide an acceptable lower bound of the fatigue life.

A summary of methods of analysis is beyond the scope of this chapter. Rather a resume of the applications of fracture mechanics to the fatigue failure of tendons is intended. It is also hoped to provide data which will be of use to the designer. Classical aspects of this section are based on two excellent reviews by Tilley [79,80]. The fracture mechanics approach uses data from Lovegrove and Salah [68–70] for reinforcing steels and from the author's laboratory for prestressing steels [30,71,72].

Fatigue crack initiation. It has been shown for many materials that there exists a critical value of the stress intensity factor range below which fatigue cracks either remain dormant or grow extremely slow at experimentally undetectable rates. This threshold cyclic stress intensity range, ΔK_{th}, is often defined as the maximum ΔK value at which no detectable growth occurs in 10^7 cycles. Since crack length monitoring equipment is usually accurate to better that 10^{-4} m, a test endurance of 10^7 cycles gives a maximum growth rate of 10^{-11} m./cycle.

Several methods have been used to establish these threshold values experimentally. The traditional approach to design under cyclic loading has involved S–N (stress range versus number of cycles to final failure) data. This approach does not separate out crack initiation and propagation stages and cannot be applied to the determination of structural life-expectancy with a crack-like defect of a known size. Nevertheless, it is accepted that for low amplitudes, some 90% of the total fatigue life is expended in developing the initial intrusion and these results can be used to estimate fatigue crack initiation as well as to establish lower limits to fatigue performance. The next section considers some results from Tilley's reviews [79,80].

Of the various types of fatigue assessment, uniaxial tests conducted on uncladded bars in repeated tension give the most conservative fatigue data. However, bending tests on reinforced concrete beams more closely reproduce service conditions and give a realistic assessment of the effect of factors that are influenced by the concrete. Each type of testing has merit and the selection of the one or the other is a question of convenience in relation to the aspect of fatigue being studied rather than any more fundamental issue. The slightly longer lives for bending tests can be justified because the highest stresses are restricted to the parts of the bar

TABLE 5.1
Values of K ($\times 10^{26}$) [80].

Type of loading	16 mm diameter	32 and 40 mm diameter
Axial	7.5	1.1
Bending	30.9	3.1

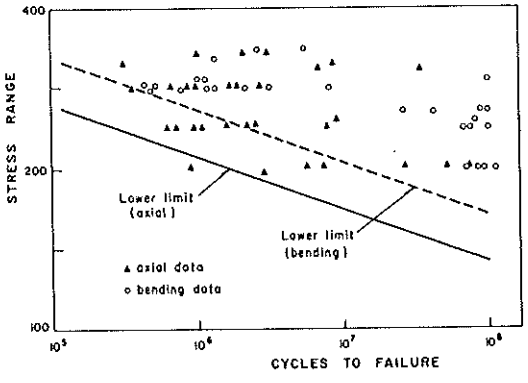

Fig. 5.23. Fatigue performance of 16 mm bars, according to G.P. Tilly and D.S. Moss [80].

furthest from the neutral axis and in the vicinities of cracks in the concrete. The likelihood of these locations coinciding with the worst defects in the bars is lower than in axial tests in which the bar is subjected to a uniform nominal stress so that fracture may be initiated from the worst defect.

The long endurance fatigue behaviour of six types of high strength reinforcement bars (cold-worked and hot rolled) has been studied and quantitative relationships involving the main variables have been evaluated. The performances have been expressed by a power law [80].

$$S^m N = K \tag{5.15}$$

When S is expressed in N/mm^2, the value of m has been shown to be close to 9. This holds for both axial tests in air and bending in concrete. The values of K are shown in Table 5.1, depending on type of test and bar characteristics.

Results of axial as well as bending test [80] are shown in Figure 5.23. A regression analysis of log N on log S was performed and a lower 95% confidence limit is shown in the figure. There is no evidence of the fatigue limit which is usually considered to develop at about 2×10^6 cycles.

Fatigue strength is dependent on the type of reinforcement bar and this is thought to be due to differences in initiation times. Plain bars with smooth surfaces exhibit the highest strengths. The presence of ribs introduces high local stresses and reduces the crack initiation phase. An increase in diameter of deformed bars produces a very pronounced reduction in fatigue strength which is an order of magnitude more than the size effect associated with plain cylindrical specimens; the strength at 10^7 cycles for 40 mm, diameter is about 25% less than for 16 mm. The explanation usually given for size effects is that bigger sections have a statistically greater likelihood of containing large flaws. For plain specimens most of the life is spent in initiation and the differences in propagation times for different diameter sections are minimal. For ribbed bars the initiation phase is reduced due to the presence of local stress concentrations at the ribs. Furthermore, Gurney [44,45] has shown that in the vicinity of a stress concentration the minimum size of flaw required to permit crack growth reduces with increased thickness of specimen. In consequence it can be argued that the initiation life of larger diameter bars is reduced.

Experimental S–N curves have been obtained for prestressing steels and Goodman or Smith diagrams may be obtained from these. As already mentioned, interpretation is made difficult when initiation and propagation times are difficult to separate. They do, however, provide much useful information for the designer.

A theoretical approach based on the concepts of fracture mechanics has been used by Lovegrove and Salah [68,69,70] and Verpoest [85] to predict crack initiation. Experimental work on formation of fatigue cracks in Torbar [68] has shown that cracks normally initiate at the root of the transverse ribs on the surface of the bar. At the peak of the first load cycle a plastic zone may be formed at the root of the rib. According to the abovementioned authors [69] the maximum depth of this zone in the bar, a_p, depends on the peak nominal stress σ_{max}, the stress concentration factor K_t the radius of the rib root ρ and the yield stress of the steel σ_y and can be estimated by the following expression:

$$a_p = \frac{\rho}{4}\left(\frac{k_t \sigma_{max}}{\sigma_y}\right)^2 - 1 \tag{5.16}$$

The critical fatigue crack is assumed to form at the deepest irregularity at the root of the rib, a_r (values of $a_r = 0.07$ mm, have been quoted [70] for Torbar steel). The initial size of the crack, a_0, may be defined as

$$a_0 = a_p + a_r$$

Therefore, the fatigue crack initiation life is defined here as the number

of cycles required to sharpen the trough of the deepest surface irregularity in the vicinity of the rib and/or damage the plastic zone. The fatigue crack initiation life, N_i, is assumed to be related to the range of the stress intensity factor ΔK_0 at the tip of the initial crack by the following equation

$$N_i = B_1(\Delta K_0)^{m_1} \tag{5.17}$$

in which B_1 and m_1 are material constants which have been evaluated [70] for Torbar steel and found to be: $B_1 = 1.448 \times 10^8$ and $m_1 = 2.701$, when MN and m units are used. No similar values are yet available for other reinforcing steels.

Fractographic examination indicate that fatigue under axial loading tends to initiate at surface defects rather than in the vicinity of the ribs. This contrast with the behaviour under bending fatigue which exhibited fractures having initiation associated with the ribs [80].

An investigation, currently in progress in the author's laboratory, suggests that the ΔK_0 range for prestressing steels is a function of the stress ratio $R = \sigma_{min}/\sigma_{max}$. For example, values of $\Delta K \simeq 20$ MN m$^{-3/2}$ for $R = 0.28$, $\Delta K \simeq 11$ MN m$^{-3/2}$, for $R = 0.67$ and $\Delta K_0 \simeq 8$ MN m$^{-3/2}$ for $R = 0.9$ have been obtained, for 7 mm diameter wires with $\sigma_{0,2} = 1400$ N/mm^2 and ultimate tensile strength of 1620 N/mm^2.

Verpoest et al. [85] have developed a model which allows a qualitative and quantitative explanation of the influence of surface characteristics and bulk properties on the fatigue limit (i.e. the maximum stress amplitude at which cracks, that are present before or created during the fatigue test, do not grow up to final fracture) and fatigue threshold were measured on 2 mm diameter wires ranging from $\sigma_n = 1320$ N/mm^2 to $\sigma_n = 2218$ N/mm^2. In this range, fatigue thresholds decreases almost linearly from 7 MN m$^{-3/2}$ to 3.5 MN m$^{-3/2}$.

Fatigue crack propagation. For many materials the rate of fatigue-crack growth can be expressed by the Paris-Erdogan equation

$$\frac{da}{dN} = C(\Delta K)^n \tag{5.18}$$

where, N is the number of cycles, C is a material constant and n is an exponent, usually about 3. Recent research has demonstrated that in a typical log-log plot of fatigue crack growth rate da/dN versus stress intensity factor range ΔK, the abovementioned law is only valid for the intermediate range of growth rates, typically $10^{-8} - 10^{-6}$ m/cycle. The variation of growth rate da/dN with ΔK is actually sigmoidal in form,

defined in a range of ΔK values bounded at its extremes by K_{IC} and threshold parameter ΔK_0.

The results of fatigue tests under constant amplitude load on cracked specimens taken from Torbar have shown that the rate of fatigue crack propagation da/dN may be described by a bi-linear relationship, to take into account the behaviour of very small cracks:

$$\frac{da}{dN} = C_1(\Delta K)^{n_1} \quad \text{for} \quad \Delta K < 9\ \text{MN.m}^{-3/2} \tag{5.19a}$$

$$\frac{da}{dN} = C_2(\Delta K)^{n_2} \quad \text{for} \quad \Delta K > 9\ \text{MN.m}^{-3/2} \tag{5.19b}$$

where, material constants are given Table 5.2.

The above theory, crack initiation plus crack propagation, was used to generate theoretical S–N data for concrete beams reinforced with Torbar. It was found [69] that the theory represents a reasonable lower bound for all the experimental data. In order to demonstrate the use of the theory, to investigate the effect of individual factors on fatigue performance of reinforced concrete beams, tests have been performed in which each of the influencing factors was varied individually. It was found that the stress concentration at the root of the rib is the most effective factor in explaining the variation in performance, 1% increase in the stress concentration factor at the rib results in 1.4% decrease in the fatigue limit at 10^7 cycles. The second most effective factor is the yield strength of the bar, indicating that provided the initiation and propagation properties of the steel are constant, improvement in the yield strength can improve the fatigue performance of the bar. Surface roughness, as measured by the maximum depth of surface irregularities, and the minimum stress have approximately identical effects, 1% increase results in about 0.15% decrease in the fatigue limit at 10^7 cycles. Minimal effects due to the change in bar size were detected. It is emphasized that the same is not true for initiation.

Experimental results of fatigue crack growth in eutectoid cold drawn steels for prestressing concrete [71] fit Paris law over a wide range of ΔK, as shown in Figure 5.24. Values of material constants are given in Table 5.2.

Figure 5.25 contains results obtained at different frequencies, with different waveforms and with different stress ratios. It seems that fatigue crack growth for prestressing steel wires is independent of waveform and frequency, at least inside the tested intervals. Crack growth also appears to be independent of stress ratio R, for positive values of R.

Integration of Paris law has been used for life prediction of prestressing wires without any defect except those produced during steel

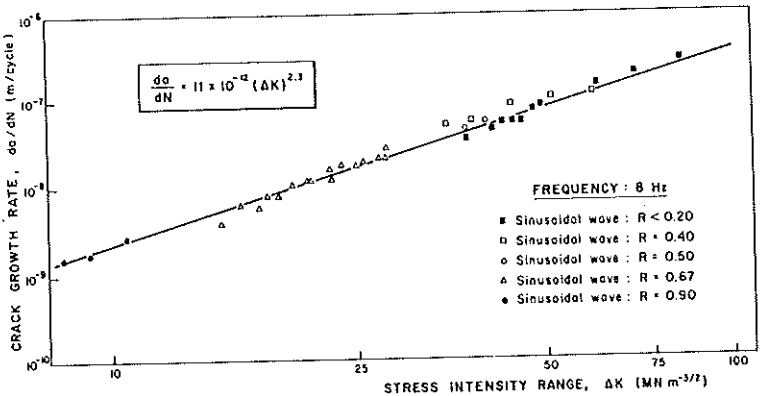

Fig. 5.24. Crack growth rate for different R values.

TABLE 5.2
Values of C and n (Units: m, MN).

Steel	$\sigma_{0.2}$ (N/mm^2)	C	n	References
Torbar	435	3.83×10^{-29}	20.9	[70] *
Torbar	435	3.16×10^{-12}	3.1	[70]
Cold-drawn	1400	11.08×10^{-n}	2.3	[71]
Cold-drawn	1520	13.96×10^{-12}	2.3	[71]
Cold-drawn	1560	16.05×10^{-12}	2.3	[71]

* For $\Delta K < 9$ MN.m$^{-3/2}$

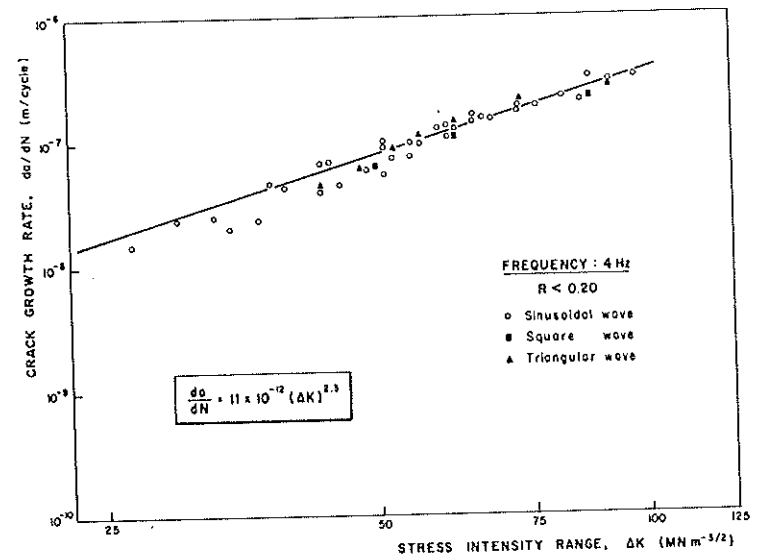

Fig. 5.25. Crack growth rate for different wave forms and frequencies.

processing. Fatigue tests results, carried out on smooth samples [30] with stress ranges high enough to ensure that initiation times are negligible as compared with propagation times, have been predicted successfully [71]. The agreement found with theoretical predictions seems to validate this approach, based on LEFM, although some plasticity has been developed, this aspect deserves further research. Another aspect, worthy of study, is the effect of material anisotropy, which has already been mentioned in the section on the fracture of cracked specimens.

Literature on fatigue failure of cables is scarce. Birkenmaier [15,16] presented a method of determining a safe value for the permissible stress range in large parallel wire tendons based on a series of systematic fatigue tests on the wire alone. Basu and Chi [13] investigated, using the methodologies of LEFM, the fatigue behaviour of bridge cables resulting from the stress reversals caused by vortex shedding. An attempt was made to compare the results of fatigue life obtained from the formulation with the available experimental data.

There is, likewise, little published information on the role of anchorages in the fatigue problem, even though these are known to be weak points [15,30]. At present, such problems are tackled empirically, there being no available theoretical treatment of fatigue in multiaxial stress systems.

There has been comparatively little work on random fatigue of reinforcement bars. The only reports the writer is aware of are the reviews of Tilly [79,80] and references therein. The section continues with a brief summary of the ideas contained in them. In this work, random loading data are expressed in terms of r.m.s. stress ranges so that they can be compared with constant amplitude data. This is based on assumptions that there are no interactive effects between different stress levels, life is wholly in propagation, and $n = 3$.

Axial tests have been performed on reinforcement bars subjected to narrow-band random loading having an approximated Rayleigh spectrum. The spectra was characterized, for convenience, by the RMS values of stress and it was realized that estimation of behaviour under variable-amplitude loading using the Palmgren-Miner concept was strongly dependent, for welded joints, on the method used to represent constant-amplitude data at long endurances. Taking an endurance limit at 2×10^6 cycles gives an optimistic or upper bound representation. Assuming the same law, $S^m N = K$, for all endurances, gives a pessimistic or lower-bound. It seems appropriate to use $S^m N = K$ to 10^7 cycles with the stress exponent raised to $m + 2$ at $N > 10^7$, because it has been shown that, for welded joints as well as for continuous bars, this gives a reasonable allowance for the contribution of low stresses which become damaging after some crack propagation has occurred.

5.5 Environment sensitive cracking

When steel is completely surrounded by concrete it may be expected that it is unlikely to suffer corrosion. Nevertheless, the ingress of aggressive ions at defects in the concrete may result in a breakdown of the passivity promoted by the relatively high pH environment that would otherwise exist. The high strength of steel for prestressing concrete, coupled to the high tensile stress to which it is subjected, raise questions as to the possibility of stress corrosion cracking since a wide range of high strength steels are well known to be susceptible to stress corrosion, particularly in the presence of chloride ions, which are found in many applications of concrete structures. Indeed, fractures thought to be due to stress corrosion have been reported in a wide range of prestressed components. Most of this information is to be found in the proceedings of three symposia organised by F.I.P. [14,18,32], a monograph by CUR [26] and reviews by Phillips [60] and Nurnberger [55].

Despite this evidence, the situation is by no means alarming and in the last F.I.P. symposium it was concluded that: "In well designed and detailed structures, which are constructed with sufficient case, the necessary conditions for stress corrosion to occur should not exist". Nevertheless, laboratory investigations have shown that prestressing steel may fracture by stress corrosion in environments that may occur when steel is unprotected by concrete. Under these conditions all steels are susceptible to stress corrosion cracking.

Thus, since a potential problem exists some comment should be made on the fracture of the steels. The section will then continue with reviews of the two most characteristic aspects of environment sensitive cracking; stress corrosion and corrosion fatigue.

Stress corrosion cracking. Just as had been the case in fatigue, the study of stress corrosion cracking in reinforcing and prestressing steels passed, first, through an empirical stage in which experimental data were accumulated and, now, it is approaching the stage where fracture mechanics can be used to obtain a more quantitative description of the phenomenon.

Experiments performed in the first phase consisted of subjecting the tendons to a predetermined load, immersing in an aggressive medium and recording the time to failure. In this way stress-time to failure curves were obtained for different media. These curves, which are analogous to S–N fatigue curves, provide much useful information on material behaviour but, just as in fatigue, there are difficulties in separating times for crack initiation and propagation. Consequently test results tend to show a lot of scatter, Figure 5.26, and the test method proposed by the F.I.P., for the detection of hydrogen embrittlement, then requires a minimum of

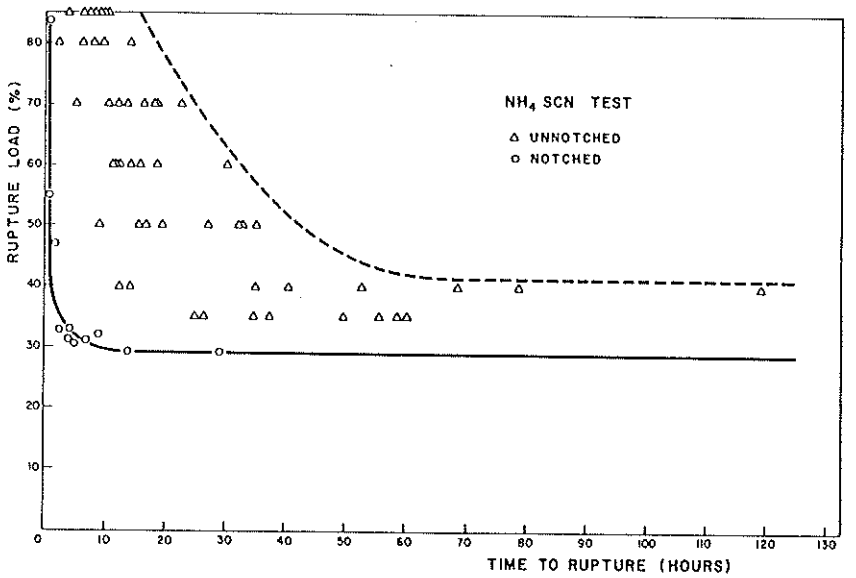

Fig. 5.26. Stress-time to fracture results for smooth specimen.

twelve specimens [39]. The tests are, however, simple, easy to perform, relatively cheap and provide much useful information [19]. For example the F.I.P. test in NH_4SCN is useful for characterizing the sensitivity of prestressing steels to hydrogen embrittlement and can be recommended for quality control of a given steel grade and to compare various prestressing steels of the same grade. Parkin's constant strain rate test [58] has also provided much valuable data on stress corrosion in prestressing steels.

The application of fracture mechanics techniques, although promising, is not without its difficulties. As well as the usual requirement of linear elasticity, there is also the need to incorporate new electrochemical parameters such as the pH of the medium and the potential between the tendon and a reference electrode. The mission of one of these has produced confusion by attempting to compare results under different conditions. The stress field in a cracked specimen is well defined by the stress intensity factor K. Bearing in mind that, at the tip of the crack, local variations in pH and potential may occur, it might be more meaningful to examine phenomena in a (K, pH_e, E_e) space, where the subscript e refers to local values, rather than in a global (K, pH, E) space.

As well as the difficulties in determining times to initiate and propagate cracks there is the additional problem of defining an initial crack size a_0. Results on cold drawn eutectoid steels [58] show that further

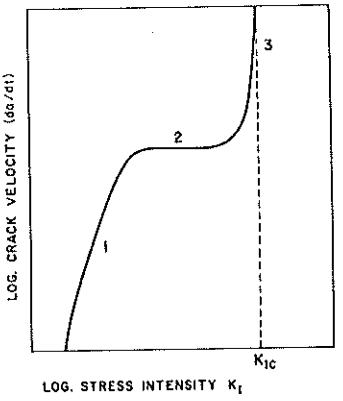

Fig. 5.27. Crack velocity versus stress intensity.

complexity is added by the presence of variables pH and E. Even under identical conditions of stress and pH, the initiation times vary with potential E; enhanced cracking results at potentials below about -900 mV (SCE), with an intermediate region in which cracking is absent or less severe than at other potentials. Cracking at higher potentials occur when the pitting potential is exceeded and appears to be dissolution-related. The surface condition, clearly, must play an important part in determining the initiation time and it has been shown that residual fabrication stresses can exert an enormous influence upon the crack initiation time, t_i [35].

The propagation phase is easier to investigate. It is known that the da/dt versus K curve can be characterised by three regions, just as in fatigue, Figure 5.27. In the first region, for K values close to K_{ISCC}, there is a rapid variation of the crack propagation rate with K. Then, in the second phase, this is much reduced and may even be insignificant. This would seem to be the case in quenched and tempered steels and, in general, in those steels which show weak anisotropy in fracture. Finally, in the third zone, in which K approaches the critical value, the growth rate increases once again until fracture. In heavily cold worked steels the crack propagation is hindered by the anisotropy of the tendon. The crack, then, tends to leave the plane perpendicular to the edge and propagate in a plane parallel to the edge. From the point of view of strength, this may be regarded as advantageous; the increase in strength being caused by a reduction in the stress intensity factor.

A number of papers have been published on this topic [20,34,52,53] and all have included experiments on tendons with transverse cracks which have been grown from notches by fatigue. The stress intensity factor, used under linear elastic conditions, has been described in Section 5.2. The K_c values were obtained by fitting a curve to data from tests in

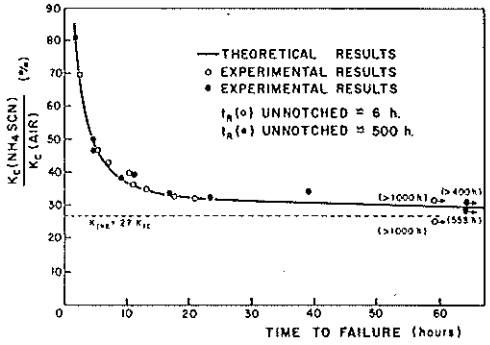

Fig. 5.28. Stress-time to fracture results for cracked specimens.

air giving failure load as a function of a/D also described earlier. One conclusion that may be drawn is that cracked prestressing steels behave in a very similar manner under test. Thus, two steels which have times to failure as different as 500 and 5 hours, as measured in the F.I.P. test, behave in an identical manner when tested with a crack, Figure 5.28. Furthermore, it has been shown that the limiting value in NH_4SCN is practically constant for all commercial steels and is of the order 30% of K_c. This limit is a function of the hydrogen fugacity which varies from one medium to another [53]. A knowledge of these limiting values in practical media would allow a determination of the design life of a prestressed member subjected to such aggressive media. While detailed work has not yet been done to establish limiting environmental conditions for cracking, it seems that these might be expected to be broadly similar to those previously found for axially precracked specimens [52] despite the pronounced anisotropy of this material.

Corrosion fatigue. Although fatigue has not proved to be a problem to date, loading cycles and corrosive conditions are becoming increasingly severe so that the margin of reserve strength is progressively being reduced. Nowadays, it is widely accepted that fatigue failure of off-shore concrete structures would most likely occur in the reinforcement tendons. Browne and Domone [21] state that, in composite reinforced or prestressed concrete – sections, the levels of the stress in the steel are a greater percentage of the ultimate stress than for concrete and it is therefore generally sufficient to consider fatigue properties of the steel as controlling the fatigue performances of the structural element.

Just happened with fatigue and stress corrosion, this problem has been tackled in a classical manner and it is only recently that it has been viewed in the light of fracture mechanics. The traditional investigation involved fatiguing beam in aggressive media, almost always seawater, and

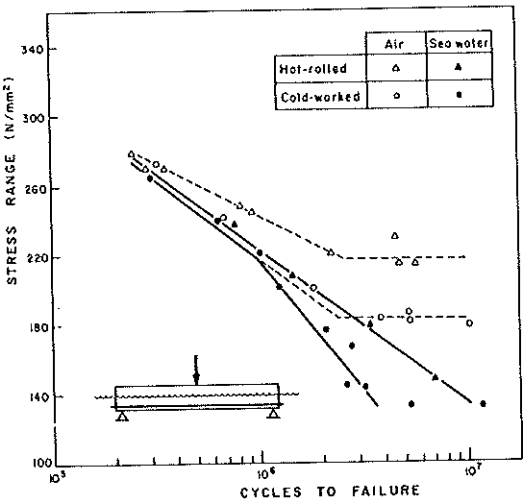

Fig. 5.29. Corrosion fatigue of steel for reinforcement. S-N curves.

recording the number of cycles to failure. A number of articles which follow this approach have been published recently [3,10,59,78]. Bending tests in a liquid environment can present experimental difficulties because it has been found that the overall stiffness of a reinforced beam increases during cycling so that stresses in the reinforcement cannot be calculated accurately [59]. This is believed to be due to cracks being wedged open by debris, a mechanism which does not occur during tests in air. A more recent paper, by Roper [65], studies the effects of differences in materials and exposure conditions on the fatigue endurance of reinforcing steels by testing reinforced concrete beams, simply supported and centrally loaded (Figure 5.29). All the beams, reinforced with hot-rolled steel, tested in sea water as well as NaCl solution (3%), showed no endurance limit before 10^7 cycles, as is suspected for corrosion-fatigue phenomena. The behaviour for beams manufactured with cold-worked steel reinforcement is not so clear and it was reported that a finite life region, with two different slopes, is followed by a long life region. Galvanizing improved the fatigue properties of concrete beams in all cases. For beams tested in air, the existence in the case of galvanized reinforcement of long life regions at higher stress ranges is noteworthy but most significant are the improvements in fatigue properties when beams are tested in the presence of sea water.

Once again, application of fracture mechanics concepts to the problem of corrosion fatigue, in this case, leads to difficulties in separating the periods of initiation from those of propagation; especially the lack of precision in the meaning of initiation. The electrolyte plays a decisive

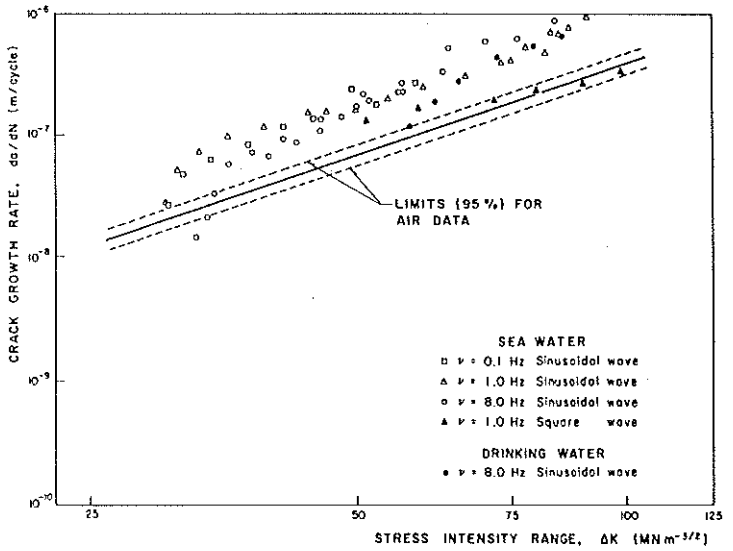

Fig. 5.30. Corrosion fatigue of prestressing steel. Crack growth rate.

part in crack initiation; so much so that it is believed that initiation will always occur, i.e. $\Delta K_0 = 0$, and that it is just a matter of waiting long enough. It should be remembered that, during its working life, a structure could suffer 10^8 cycles. Crack initiation time is reduced as corrosion pits readily become initiation sites for fatigue cracks. Pit development is time dependent rather than frequency dependent; the longer the corrosion fatigue life, the greater the reduction in fatigue endurance.

The pattern of crack growth rate in corrosion-fatigue is not so simple as in fatigue or stress corrosion alone. The effect of the corrosive medium is to increase the fatigue crack growth rate and this can depend on frequency, wave form and stress ratio, R, among other parameters. Recent, as yet unpublished results [72] for prestressing steels are shown in Figure 5.30. These are based on 7 mm diameter, cold drawn eutectoid steel with a $\sigma_{0.2} = 1400$ N/mm^2. The experiments were performed on precracked tendons with crack depths ranging from 1.5 to 3.5 mm. As may be deduced from the figure, the rate of crack propagation increases in a liquid medium such as in seawater or drinking water. Effects of frequency are rare or insignificant in the range 0.1 to 8 Hz. There does, however, seem to be a detectable effect of wave form and values obtained with a square wave are similar to those in air.

The advantages of the treatment of corrosion fatigue with fracture mechanics techniques are still to be realised in current design codes. So that both API [1] and F.I.P. [38] state that the resistance of a structure is adequate, if the stress range in the straight rebars is less than 140

N/mm^2. FIP also imposes a minimum stress level of 0,4 σ_y. Veritas [28] specifies both a Wohler curve and an endurance limit. With these criteria, allowing more cycles in the useful design life of the structure would require the specification of lower endurance limits.

References

1. ACI Report 357R-78, Guide for the design and construction of fixed offshore concrete structures, American Concrete Institute (1978).
2. Ammann, W., Muhlematter, M., Bachmann, H., Stress-strain behaviour of non-prestressed and prestressed reinforcing steel at high strain rates. Symp. Concrete Structures under impact and impulsive loading. RILEM.CEB.IABSE.IASS. Bundesanstalt fur Materialprufung (BAM) (1982).
3. Arthur, P.D., Earl, J.C. Hodgkiss T., Fatigue of reinforced concrete in sea water, Concrete. Vol. 13, n° 5 pp. 26–30 (1979).
4. Astiz, M.A., Estudio de una fisura superficial en un alambre de acero de alta resistencia, Universidad Politécnica de Madrid. Escuela de Ingenieros de Caminos (1976).
5. Astiz, M.A., Elices, M., Morton J., Valiente, A., A photoelastic determination of stress intensity factors for an edge-crack rod in tension, Proceedings Soc. Exp. Stress Analysis. Michigan Meeting (1981).
6. Astiz, M.A., Elices, M., An elastic singularity element for two and three dimensional crack problems (to be published).
7. Athanassiadis, A., Stabilité, tenacite, propagation des fissures dans les fils et barres en acier, Report de recherche LPC 89 (1979).
8. Ayling, E., Bevan, L., Load distribution in a single-edge-notch tensile specimen, Int. J. Fracture Mech. 8 pp. 341–342 (1972).
9. Bannister, J.L., Steel reinforcement and tendons for structural concrete, Concrete, July, August (1968).
10. Bannister, J.L., Fatigue and corrosion fatigue of Tor bar reinforcement, The Structural Engineer. Vol. 56 A, pp. (1978).
11. Bartos B. (Ed.), Bond in concrete, Applied Science Publishers pp. 466 (1982).
12. Barker, L.M., Short rod and shor bar fracture toughness specimen geometries and test methods for metallic materials, ASTM STP 743 pp. 456–475 (1981).
13. Basu, S., Chi, M., Analysis study for fatigue of bridge cables, IABSE Colloquium. Fatigue of steel and concrete structures Lausanne 1982.
14. Bijl, C.L., Lamers, L.R., Wind, G. (Eds), 1st FIP stress corrosion symposium, Royal Dutch Blast Furnaces and Steelworks Ltd. (1971).
15. Birkenmaier, M., Narayab R., Fatigue resistance of large high tensile steel stay tendons, IABSE Colloquium. Fatigue of steel and concrete structures Lausanne 1982.
16. Birkenmaier, M., Fatigue resistance tendon for cable-stayed construction, IABSE Proceed. P.30/80, May 1980.
17. Blackburn, W.S., Calculation of stress intensity factors for straight cracks in grooved and ungrooved shafts, Eng. Fracture Mechanics, Vol. 8 731–736 (1976).
18. Blekkenhorst, F., Lamers, L.R., Wind, G. (Eds), 2nd. FIP stress corrosion symposium, Hoogovens IJmuiden, B.V. (1974).
19. Brachet, M., Bilan de quelques années d'observation des phenomenes de corrosion sous tension des fils en acier a hautes caracteristiques, Annales de l'ITBTP vol. 267. pp. 81–100 (1970).

20. Brachet, M., Raharinaivo, A., Stress corrosion cracking of reinforcing bars, Int. Conf. SCC and HE of iron base alloys. NACE pp. 766–773 (1973).
21. Browne, R.D., Domone, P.L., Permeability and fatigue properties of structural marine concrete at continental sheef depths, Int. Conf. Underwater Construction Technology. Cardiff (1875).
22. Bush, A.J., Stress intensity factors for single-edge-crack solid and hollow round bars loaded in tension, J. Testing and Evaluation, JTEVA, Vol. 9, n° 4, 216–223 (1981).
23. CEB Bond action and bond behaviour of reinforcement, Bulletin d'information N 151 (1982).
24. CEB Design of concrete structures for fire resistance, Bulletin d'information N. 145 (19) (1982).
25. Creager, M., Paris, P. Elastic field equations for blunt cracks with references to stress corrosion cracking, Int. J. Fracture Mechanics, Vol. 3 n°4. pp. 247–252 (1967).
26. CUR, Cases of damage due to corrosion of prestressing steel, Netherlands Committee for Concrete Research pp. 96 (1971).
27. Daoud, O.E.K., Cartwright, D.J., Carney, M., Strain energy release rate for a single-edge-cracked circular bar in tension, J. Strain Analysis. Vol. 13, n°2, 83–89 (1978).
28. Det Norske Veritas, Rules for the design, construction and inspection of offshore structures, Appendix D. Concrete Structures (1977).
29. Dixon, J.R., Strannigan, J.S., McGregor, J., Stress distribution in a tension specimen notched on one edge, J. Strain Analysis, Vol. 4, n° 1, pp. 27–31 (1969).
30. Elices, M., Sánchez-Gálvez, V., Fatiga de alambres de pretensado, Hormigón y Acero, V. 125, pp. 85–99, 1977.
31. Elices, M., Mestre, A., Planas J., Valiente, A., Low temperature fracture properties of steels for reinforcing and prestressing concrete (to be published).
32. Elices, M., Sánchez-Gálvez, V., 3rd, FIP stress corrosion symposium, FIP and Berkeley Univ. (1982).
33. Elices, M., Faas, W., Rostasy, F., Wiedemann, G. Cryogenic behaviour of materials for prestressed concrete, FIP/5/11 84 pp. (1982).
34. Elices, M., Sánchez-Gálvez, V., Entrena, A., SCC testing of cold drawn steel wires in NH_4SCN solution. K_{ISCC} measurements, 3rd FIP Symposium on stress corrosion (1982).
35. Elices, M., Maeder, G. and Sánchez-Gálvez, V. Effect of surface stress on hydrogen embrittlement of prestressing steels, Br. Corros. J., Vol. 18, No. 3 (1983).
36. Fan Yuan-Xun, Tian-you Fan and Da-Jun Fan, The approximate analytical solution for both surface and embedded cracks in cylinder with finite size, Eng. Fracture Mech. Vol. 16 n° 1, pp. 55–67 (1982).
37. FIP, Report on Prestressing steel: 1, types and properties (1976).
38. FIP, Recommendations for the design and construction of offshore sea structures, FIP Recommendations (1977).
39. FIP, Report on Prestressing Steel: 5. Stress Corrosion Cracking resistance test for prestressing tendons (1980).
40. Godfrey, H.J., The fatigue and bending properties of cold-drawn steel wire, Trans. ASM, pp. 133–168 (1941).
41. Godfrey, H.J., Compression and tension test of structural alloys (Discussion), Proceed. ASTM Vol. 41, pp. 573–574 (1941).
42. Godfrey, H.J., The mechanical properties of steel wire: A seminar, The Wire Association International (1979).
43. Goto, Y., Miura, T., Experimental studies on properties of concrete cooled to about −160°C, Tohoku University Report. Vol. 44, n° 2 pp. 357–385 (1979).
44. Gurney, T.R., The influence of thickness on fatigue strength of welded joints, Proceed. 2nd Int. BOSS Conf. pp. 523–534 (1979).

45. Gurney, T.R., Johnston, G.O., Revised analysis of the influence of defects on the fatigue strength of transverse non load carrying fillet welds, Welding Res. Inst. 3 pp. (1979).
46. Hahn, G.T., Sarrate, M., Rosenfield, A.R., Criteria for crack extension in cylindrical pressure vessels, Int. J. Fracture Mechanics, Vol. 5 pp. 187–210 (1969).
47. Hobbs, R.E., Ghavami, K., The fatigue of structural wire strands, Int. J. Fatigue pp. 69–72, April 1982.
48. Knott, J.F., Fundamentals of Fracture Mechanics, Butterworths, pp. 153, 1973.
49. Kong, B. Paris, P.C., On the cup and cone fracture of tensile bars, ASTM STP 677 pp. 770–780 (1979).
50. Limberger, E., Brandes, K., Herter, J., Influence of mechanical properties of reinforcing steel on the ductility of reinforced concrete beams with respect to high strain rates, Symp. Concrete Structures under impact and impulsive loading, RILEM.CEB. IABSE. IASS, Bundesanstalt fur Materialprufung (BAM) (1982).
51. Maupetit, P., Olivie, F., Raharinaivo, A., Francois, D., Shear fracture of prestressing plain carbon steel wires under complex loading, Int. J. Fracture, pp. 725–727 (1977).
52. McGuinn K.F., Griffiths J.R., Rational test for stress corrosion crack resistance of cold drawn prestressing tendon, Br. Corros. J., Vol. 12 No. 3, pp. 152–157 (1977).
53. McGuinn, K.F., Elices, M., Stress corrosion resistance of transverse precracked prestressing tendon in tension, Br. Corrs. J. Vol. 16, pp. 187–195 (1981).
54. Mestre A., Comportamiento mecânico de aceros de armar y pretensar en condiciones criogénicas, Tesis Doctoral (1982).
55. Nurnberger, U., Analyse und Auswertung von Schadensfallen and Spannstahlen Strasenbau und strasenverkehrstechnik. Heft 308 (1980).
56. Paris, P.C., Tada, H., Zahoor, A., Ernst, H., The theory of instability of the tearing mode of elasto-plastic crack growth, ASTM STP 668, pp. 5–36 (1979).
57. Parkins, R.N., Stress Corrosion cracking. The slow strain rate technique, ASTM. STP 665 (1979).
58. Parkins, R.N., Elices, M., Sanchez-Gálvez, V., Caballero, L., Environment sensitive cracking of prestressing steels, Corrosion Science. Vol. 22, pp. 379–405 (1982).
59. Peyronnel, J.P., Trinh, J., Experimental study on the behaviour of concrete structural element in sea water, Annales de l'ITBTP. Vol. 360, pp. 42–57 (1978).
60. Phillips, E., Survey of corrosion of prestressing steel in concrete water retaining structures, Australian water Resources Council. Tech. Paper n°9 (1975).
61. Raharinaivo, A., Utilisation des concepts de la mecanique de la rupture pour l'exploitation des essais classiques de corrosion sous tension. Corrosion, Traitements, Protections, Finition, Vol. 20, pp. 276–284 (1972).
62. Rehm, G., Nurnberger, U., Patzak, M., Keil und Klemmverankerungen fur dynamish beanspruchte Zugglieder and Hochfesten Drahten, Bauingenieur 51 pp. 287–298 (1977).
63. Reinhardt, H.W., Concrete under impact loading. Tensile strength and bond, Heron. Vol. 27, n°3, pp. 2–48 (1982).
64. Rogers, H.C., The effect of material variables on ductility, Ductility ASM pp. 31–62 (1968).
65. Roper, H., Reinforcement for concrete structures subject to fatigue, IABSE Colloquium. Fatigue of steel and concrete structures. Lausanne 1982.
66. Rostasy, F.S., Kepp, B., Time dependence of bond, Institut fur Baustoffe, Massivbau und Brandschutz, Braunschweig (1982).
67. Sager, H., Rostasy, F.S., The effect of elevated temperature on the bond behaviour of embedded reinforcing bars, Technische Universität. Braunschweig (1982).
68. Salah el Din, A.S., Lovegrove, J.M., Formation and growth of fatigue cracks in reinforcing steel for concrete, Fatigue of Engineering Materials and Structures, V. 3, pp. 315–323 (1980).

69. Salah el Din, A.S., Lovegrove, J.M., Fracture mechanics predictive technique applied to fatigue IABSE Colloquium. Fatigue of steel and Concrete Structures. Lausanne 1982.
70. Salah el Din, A.S., Lovegrove, J.M., Fatigue of cold worked ribbed reinforcing bar. A fracture mechanics approach, Int. J. Fatigue. pp. 15–26, January 1982.
71. Sanchez-Gàlvez, V., Elices, M., Valiente, A., Fatigue crack propagation in steel prestressing wires, IABSE Colloquium, Fatigue of Steel and Concrete Structures. Lausanne 1982.
72. Sánchez-Gálvez, V., Valiente, A., Elices, M., Corrosion fatigue of prestressing steels, III Congreso Nacional y I Iberoamericano de Corrosión y Protección, Madrid (1983).
73. Shupack, M., A survey of the durability performance of Post-Tensioning Tendons, J.ACI. Vol. 75, pp. 501–510 (1978).
74. Sih, G.C., A three-dimensional strain energy density factor theory of crack propagation, Mechanics of Fracture 2. Edited by G.C. Sih, Noordhoff International Publishing, Leyden, pp. 15–53 (1975).
75. Sih, G.C., Fracture Toughness Concept, ASTM STP 605, pp. 3–15 (1976).
76. Sih, G.C., Experimental fracture mechanics: Strain energy density criterion Mechanics of Fracture. 7, Edited by G.C. Sih, Martinus Nijhoff Publishers, pp. 17–56 (1981).
77. Suaris, W., Shah, S.P., Mechanical properties of materials, Symp. Concrete Structures under impact and impulsive loading, RILEM. CEB. IABSE. IASS., Bundesanstalt fur Materialprufung (BAM) (1982).
78. Taylor, H.P., Sharp, J.V., Fatigue in offshore concrete structures, The structural Engineer. Vol. 564, pp. (1978).
79. Tilly, G.P., Fatigue of steel reinforcement bars in concrete: A review, Fatigue of Engineering Materials and Structures. V. 2, pp. 251–268 (1979).
80. Tilly, G.P., Moss, D.S., Long endurance fatigue of steel reinforcement, IABSE Colloquium. Fatigue of steel and concrete structures. Lausanne. 1982.
81. Trotter, H.G., High strength steel reinforcement, The Metallurgist and Materials Technologist, pp. 73–76 (1977).
82. Valiente, A., Criterios de fractura para alambres, Universidad Politécnica de Madrid. Escuela de Ingenieros de Caminos (1980).
83. Valiente, A., Elices, M., Morton, J., Determinación de factores de intensidad de tensiones mediante la utilización de tecnicas fotoelasticas con modelos entallados, Anales de Física. Vol. 77, pp. 122–129 (1981).
84. Valiente, A., Elices, M., Fracture of steel wires under lateral load (unpublished results).
85. Verpoest, I, Deruyttere, A., Aernoudt, E. Neyrinck M., The fatigue limit of steel wires as determined by the fatigue threshold and the surface characteristics, Proceedings of the 4th. ECF Conference (1982).
86. Yamane, S., Kasami, H., Okuno, T., Properties of concrete of very low temperatures, ACI-SP 55 pp. 207–221 (1978).